sustainability

MDPI

Article

Socio-Economic Impacts of Pluvial Floods in the Metropolitan Area of Barcelona in a Climate Change Context

Àlex de la Cruz-Coronas [1,2,*], Beniamino Russo [2], Sofia Pacho-Gómez [1] and Daniel Yubero-Peña [1]

[1] Climate Change & Resilience Unit, Veolia, Paseo de la Zona Franca 46–48, 08038 Barcelona, Spain; sofia.pacho@veolia.com (S.P.-G.); daniel.yubero@veolia.com (D.Y.-P.)
[2] Flumen Research Institute, Universitat Politècnica de Catalunya—BarcelonaTech (UPC), and International Centre for Numerical Methods in Engineering (CIMNE), Campus Nord UPC, Jordi Girona 1–3, B0 S1, 08034 Barcelona, Spain; beniamino.russo@upc.edu
* Correspondence: alex.cruz@veolia.com

Abstract

Pluvial floods can cause severe socio-economic impacts on coastal urban areas like the Metropolitan Area of Barcelona. This study combined the development of high-resolution flood maps, based on a large-scale coupled 1D/2D model and empirical functions, to quantify direct economic damage to buildings and determine risk to pedestrians and vehicles. Importantly, the flood model included a network of 36 municipalities and covered 636 km^2. Three scenarios were considered: single-hazard (extreme precipitation), multi-hazard (coincident extreme precipitation and storm surge), and adaptation (implementation of resilience measures). In total, 20 rain events were applied for each scenario: 5 were historic design storms, while 15 considered the effect of climate change (60 simulations in total). By the end of the century, results show potential increases in expected annual damage of up to 36%, from €139.8 M to €190.3 M. Risk for pedestrians could increase by 25% (494 ha to 620 ha) and for vehicles by 26% (59 km to 75 km) in the T10 single-hazard scenario. In the multi-hazard case, the socio-economic impacts are approximately 5% higher, while the adaptation simulations considering sustainable urban drainage systems show reductions between 6 and 18%. The metropolitan results were compared and validated with a previous assessment done in the City of Barcelona. Based on these results, urban planners, emergency responders, and public administrations can develop effective adaptation measures based on cost–benefit analyses for current and future climate scenarios. Compared to previous studies, this approach adapts existing urban-scale methodologies to regional-scale flood risk assessment.

Keywords: urban floods; climate resilience; impact assessment; risk qualification; decision-making; sustainable urban development

Check for updates

Academic Editor: David Pastor-Escuredo

Received: 17 March 2026
Revised: 10 April 2026
Accepted: 21 April 2026
Published: 4 May 2026

Copyright: © 2026 by the authors. Licensee MDPI, Basel, Switzerland. This article is an open access article distributed under the terms and conditions of the Creative Commons Attribution (CC BY) license.

1. Introduction

Globally, urban floods are increasing as a consequence of climate change, which causes higher precipitation intensities and sea-level rise [1]. In parallel, growing urbanization, especially in coastal low-lying areas, raises the population and assets exposed [2–4]. As a consequence, the socioeconomic impacts of floods, particularly in urban areas, have increased over the last decades and are expected to keep growing in the future [5,6]. Floods generate significant socio-economic impacts that extend beyond direct physical damage, affecting livelihoods, public safety, and the functioning of urban systems [7–9]. Economic losses associated with building damage remain one of the most commonly quantified

impacts, typically estimated through depth–damage functions, while increasing attention has been given to indirect effects such as disruption of transport networks, loss of economic activity, and impacts on human well-being [10–12].

At the European level, it is estimated that in 2021, 12% of the continent's total population lived in flood-prone areas [13]. Consequently, between 2008 and 2023, 320,000 displaced people and 4250 casualties were associated with floods in this part of the world [14,15]. According to the European Environmental Agency, from 1980 to 2020, floods cost 450 to 520 billion euros at the continental scale. Remarkably, 60% of these losses are associated with only 3% of all events [16]. Improving preparedness to mitigate such impacts requires multi-sectoral and multi-perspective climate resilience action based on solid risk assessments of extreme weather events with a multi-hazard scope [17,18].

Urban areas have complex topographies, extensive impervious areas, and, often, aged drainage systems. This reality makes them challenging areas for pluvial flood assessments. However, significant advances in the field of hydroinformatics have allowed the development of accurate studies in urbanized contexts [19]. 1D/2D coupled models are the most adequate modeling tools for the development of urban flood assessments [20,21]. On the one hand, the 1D module computes the transport of water in the underground drainage system using the one-dimensional Saint-Venant equations [22,23]. On the other hand, the 2D module simulates overland runoff transportation based on the shallow water equations. Simultaneously, the water exchange between both domains is also computed. The outputs of these models are accurate maps of water depth and velocity in the study area [24].

These kinds of models have been widely applied to simulate inundation dynamics and support risk-based decision-making [25,26]. More recent studies have extended this framework by integrating climate change scenarios and socio-economic pathways, highlighting the importance of considering both hazard evolution and exposure dynamics when projecting future flood risk [27–29]. However, despite these advances, most applications involving 1D/2D coupled models remain limited to city-scale analyses [30,31], while regional-scale studies tend to overlook or oversimplify the effect of drainage networks [32–35].

In addition to pluvial flooding, multi-hazard flood scenarios resulting from the concurrence of intense rainfall and storm surge are particularly relevant. Coastal urban areas are increasingly exposed to such compound flooding. In these multi-hazard events marine and pluvial drivers interact nonlinearly, causing impacts that exceed those expected from individual hazards acting independently [36,37]. One of the key mechanisms in these interactions is the backwater effect in coastal drainage systems: elevated sea levels can limit or reverse the discharge capacity of urban outfalls, causing water levels to rise within the underground sewer network and the urban surface [38]. The occurrence of such compound (multi-hazard) events is expected to increase due to climate change, as sea-level rise and changes in storm characteristics amplify the probability and severity of joint coastal–pluvial extremes [39,40]. Therefore, considering multi-hazard flood drivers and their interactions is essential for robust risk assessments and supporting effective adaptation planning in coastal metropolitan regions [41].

Flood hazard maps derived from both single- and multi-hazard scenarios constitute the basis for subsequent impact assessments [25]. These results offer stakeholders, such as public authorities, infrastructure operators, and risk managers, valuable insight for better decision-making in climate adaptation.

Because of the above, the Horizon Europe ICARIA project aimed to promote asset-level modeling practices to improve the resilience of critical assets against multi-hazard events in different European regions. The Metropolitan Area of Barcelona (AMB, its acronym in Catalan) was one of them. Located in the western Mediterranean, it is a hub of economic activity and home to 3.3 million people. From a hydrologic point of view, it consists of

fluvial and coastal plains with urban and industrial areas surrounded by medium-elevation mountain areas (see Figure 1). Consequently, it has a fast hydrologic response time that can cause flash floods in the downstream plains. In addition, its typical Mediterranean weather is prone to extreme convective events. The combination of these factors makes the AMB a sensitive region for flood-related risks [42].

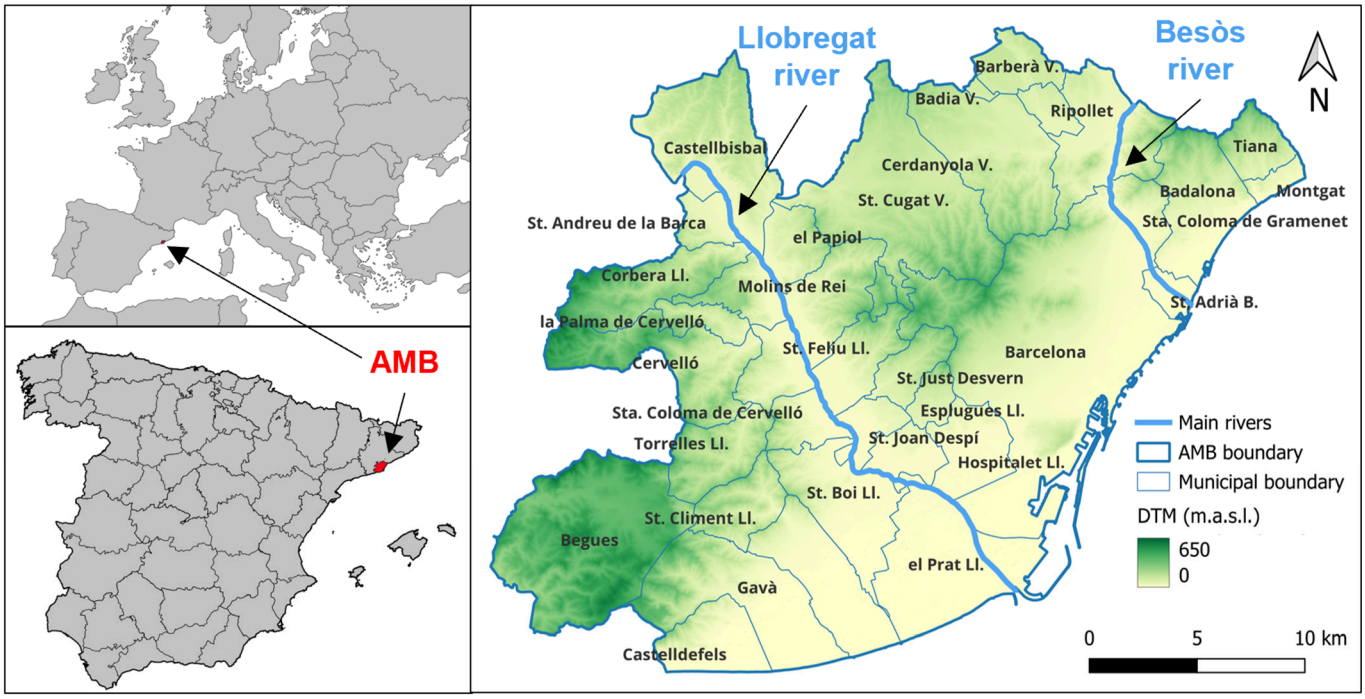

Figure 1. Location and main characteristics of the Metropolitan Area of Barcelona. Source: Authors.

The objective of this paper is to assess the effect of climate change on the socio-economic impacts of floods in the AMB for three different scenarios: (a) pluvial floods, (b) compound floods, and (c) an adaptation scenario.

Compared to previous studies, this work addresses a key gap by extending the application of highly detailed coupled 1D/2D models from the city scale to the regional scale while preserving a high level of detail in the sewer network representation. In addition, the framework incorporates a tailored vulnerability assessment that reflects the socio-economic heterogeneity of the 36 municipalities within the study area. Furthermore, the analysis integrates updated climate change projections and adopts a multi-hazard perspective of combined floods.

Indeed, flood hazard assessment is often constrained by limited data availability, including rainfall patterns, terrain characteristics, and hydrologic and hydraulic information. In response to these challenges, many recent machine learning and deep learning approaches have been developed as reliable alternatives to traditional physics-based models, even under data scarcity [43,44]. However, the present study focuses on a region with abundant data and well-established prior studies. This allows the development of a high-resolution, physics-based model capable of capturing the local complex dynamics, making alternative methods unnecessary in this work.

2. Materials and Methods

The risk assessment methodology applied followed the guidelines of the ICARIA project [45], consistent with AR6 [1] and the SENDAI framework [46]. According to the project, risk is defined as the combination of three factors:

- Hazard: time-space distribution of the severity of an event characterized by an assigned probability of occurrence in a location and timeframe.
- Exposure: distribution of risk receptors occupying a specific location and time in the area affected by the modeled hazard.
- Vulnerability: the susceptibility of exposed risk receptors to be damaged by the modeled hazard types and their intensities.

Figure 2 exemplifies how this conceptual framework was adapted to estimate flood economic damage to buildings. Hazard corresponded to metropolitan-scale flood maps produced with a 1D/2D model, indicating water depth and velocity. Exposure consisted of the location and typology of the assets of interest in the AMB. Vulnerability was assessed based on specific damage to vulnerability functions.

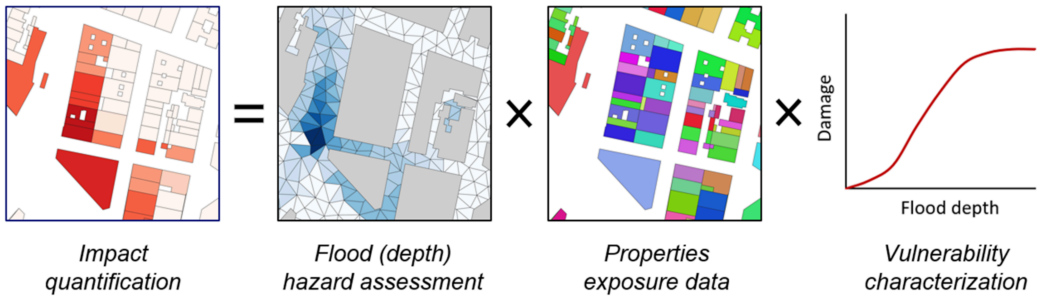

Figure 2. Risk assessment conceptual framework for urban flood impact assessment on properties. Source: Authors.

Figure 3 details how the previous conceptual framework was developed into a workflow to assess the socio-economic impacts of floods in the AMB. It indicates the data inputs, applied methodologies, used models, and result outputs.

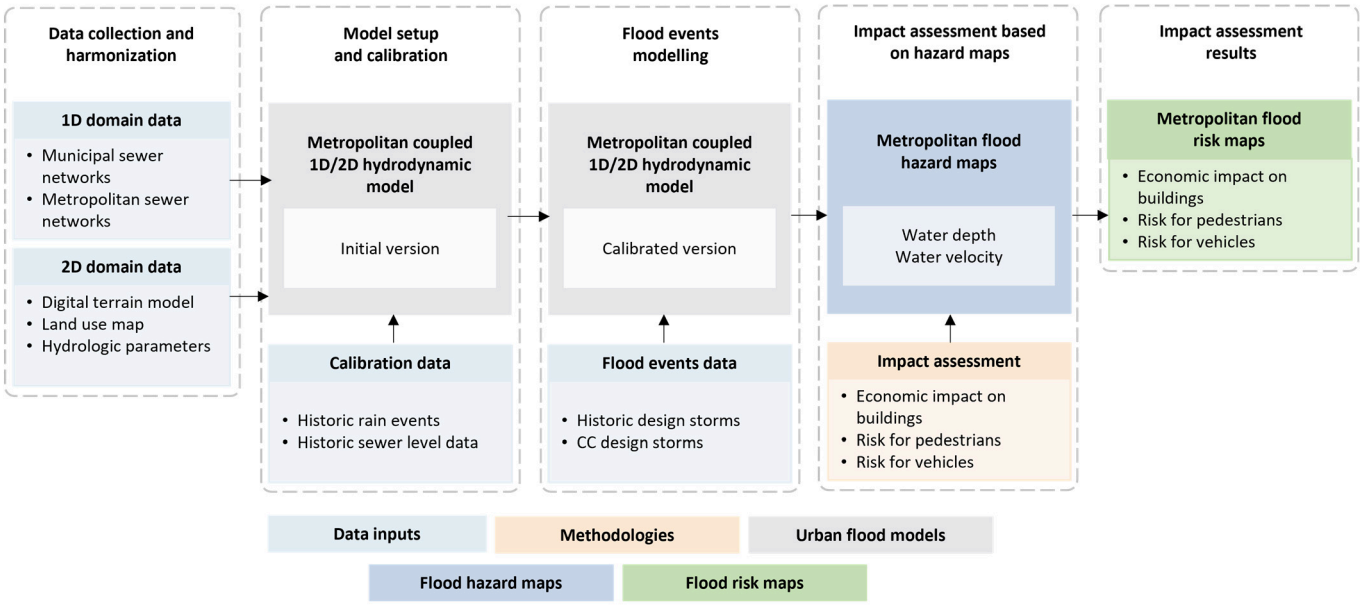

Figure 3. Workflow diagram of the urban flood impact assessment methodology implemented. Source: Authors.

2.1. Data Collection and Preprocessing

The development of this work involved extensive initial data collection. Consistent with Figure 3, Table 1 details the datasets involved, their uses in the risk assessment workflow, and their sources.

Table 1. Datasets involved in the pluvial flood risk assessment processes.

Dataset	Use	Source	Reference
Drainage sewer models (municipal and metropolitan)	1D domain of the flood model setup	Municipalities and asset operators	n.a. (private data)
Digital terrain model	2D domain of the flood model setup	Institut Cartogràfic i Geològic de Catalunya	[47]
Land-use maps			
Hydrologic parameters		RESCCUE project	[48]
Historic rain and sewer data	Flood model calibration	Asset operators	n.a. (private data)
Historic design storms	Flood simulations	Barcelona Urban Drainage Master Plan	[49]
Historic design storms	Flood simulations	Regional downscaling of climate projections	[50]
Buildings' exposure (cadastral data)	Building's risk assessment	Catastro España	[51]
Buildings' vulnerability (vulnerability curves)		Depth–damage curves	[52]
Pedestrians' exposure (population distribution)	Pedestrian's risk assessment	National Institute of Statistics	[53]
Pedestrians' vulnerability (socio-demographic data)			
Vehicles' exposure (road network)	Pedestrian's risk assessment	Open Street Map	[54]
Vehicles' vulnerability (road hierarchy)			

To ensure consistency across the different datasets in Table 1, data preprocessing was applied. First, all spatial datasets were harmonized into a common coordinate reference system and aligned to a consistent spatial resolution compatible with the 2D computational mesh. Second, several datasets were transformed into model-ready parameters. Land-use information was translated into hydrological properties, such as infiltration and roughness. Cadastral data were converted into exposure indicators, while socio-demographic data were aggregated at the census tract level. Third, the sewer network dataset was homogenized based on the parameters and nomenclature of the selected modeling software. Fourth, temporal datasets such as rainfall time series and design storms were formatted into consistent time steps and durations required by the hydrodynamic simulations. Finally, quality control procedures were applied to detect inconsistencies and ensure a coherent integration of all inputs in the coupled 1D/2D modeling environment and the subsequent impact assessment post-processes. The following section provides further detail on the workflow implementation.

2.2. Hazard Flood Model Setup

A coupled 1D/2D hydrodynamic model was developed in Infoworks Ultimate v2026.2 [55] to assess pluvial floods across the entire AMB, covering a domain of 636 km^2. The reasons for selecting this software were its robustness and capacity to perform complex 1D/2D simulations with extensive sewer networks. In addition, it is a widely used

modeling tool in the area of study. Thus, the sewer network provided by the municipalities was already compatible with this software.

The 2D domain was based on a 2 × 2 m digital terrain model and a land-use classification that assigned hydrological parameters (Horton infiltration or fixed losses) to 11 surface classes. To balance resolution and computational demand, a variable-size unstructured mesh was applied. Urbanized zones were discretized in 25–100 m^2 cells, while non-urban areas were discretized in 500–1000 m^2 cells. This resulted in a mesh of 6.8 million elements. Remarkably, the terrain discretization followed a hybrid approach [25]. Therefore, all built parcels were removed from the mesh and represented as subcatchments. Consequently, the runoff generated in building roofs was directly routed to the nearest sewer node, while rainfall was applied simultaneously to the 2D elements of the meshed surface.

The 1D domain included the local sewer networks of the AMB together with the metropolitan interceptor system, resulting in a continuous drainage model of over 4950 km of pipes and 181,000 nodes. All singular drainage infrastructures, including storage tanks, syphons, valves, regulators, and pumping stations, were also modeled based on their operational rules.

The coupling between the 1D and 2D domains was resolved through inlet-based flow exchange. All manholes were defined as "gully2D", so their drainage capacity depended on the number of associated inlets and inlet-specific head–discharge relationships derived from experimental studies, allowing a realistic assessment of drainage systems' performance in terms of runoff detention. The model incorporated all outfalls from local and metropolitan networks.

To ensure reliability, the model was calibrated and validated using high-resolution rainfall and water-level records from monitored events in Barcelona. Calibration focused on adjusting key hydrological and hydraulic parameters to improve the model performance compared to field observations. More details on the model setup process, parameters, data sources, and calibration–validation are provided in a specific report [48].

As mentioned, this study incorporated a multi-hazard perspective to assess the consequences of coincident extreme precipitation and storm surges. Figure 4 illustrates how their interaction can limit the runoff conveyance capacity of outfalls into the sea as the receiving body. Multi-hazard simulations utilized "water-level" boundary conditions for all sea-connected outfalls. These conditions represented the temporal evolution of sea levels during the simulation. If the sea level exceeded the elevation of a given outfall, its outflow capacity was reduced. Thus, the multi-hazard simulations were based exactly on the same 1D/2D model used for the single-hazard scenario, incorporating a boundary condition representing sea level.

Regarding the adaptation scenario, its objective was to test the risk-reduction capacity of a hypothetical implementation of a set of flood adaptation measures in the AMB. In terms of modeling, it involved adjusting characteristic parameters of model elements, such as the contributing areas of certain subcatchments, Manning roughness coefficients, or infiltration rates. All changes were applied to the 1D/2D model used for the single- and multi-hazard scenarios. Section 2.3.3 specifies the adaptation measures implemented and the corresponding changes in the model.

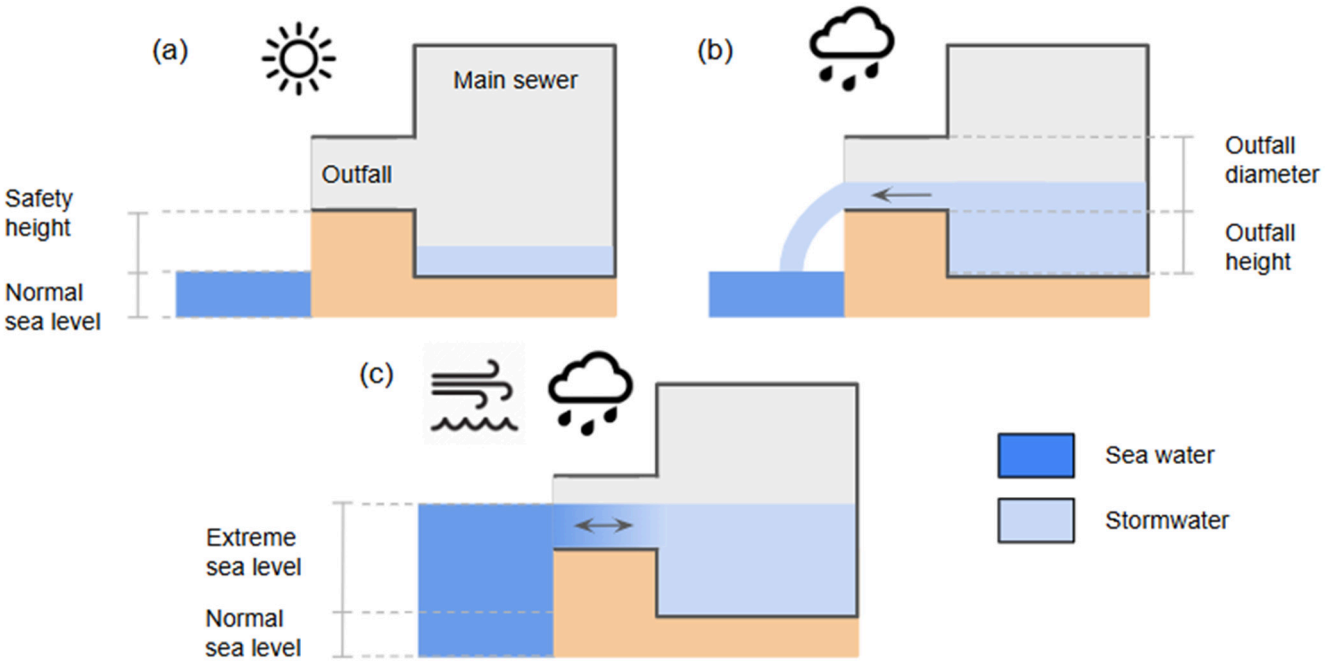

Figure 4. Scheme of backwater effect affecting urban drainage systems during (**a**) dry weather conditions, (**b**) a precipitation event, and (**c**) a coincident precipitation and storm surge with backflow occurrence. Source: Authors.

2.3. Hazard Assessment Scenarios

This section presents the climate conditions and event severity (rainfall intensity and storm surge level) considered in the flood hazard assessments performed for the three scenarios (single-hazard, multi-hazard, and adaptation).

2.3.1. Single-Hazard Scenario Simulation

The single-hazard simulations (SH) considered 20 synthetic rainfall events or design storms. Five of them represented baseline conditions and corresponded to the design storms defined in the last Urban Drainage Master Plan of Barcelona. These baseline events were derived from intensity–frequency–duration curves based on historic precipitation data of local rain gauges. The resulting hyetographs had a duration of 160 min, split into 5 min blocks, and were associated with return periods of 1, 10, 50, 100, and 500 years [49]. The other 15 rainfall events were developed to represent future climate change conditions. These scenarios were constructed by modifying the same five design hyetographs to reflect projected variations in rainfall intensity derived from deterministic, downscaled climate projections for the AMB. Specifically, the adjustments were based on the Shared Socio-economic Pathway 5–8.5 emissions scenario as a worst-case benchmark. Three future projection periods were considered: short-term (Period 1, 2015–2040), medium-term (Period 2, 2041–2071), and long-term (Period 3, 2071–2100) [50]. The adjustment to the future climate projections was based on the statistical downscaling of an ensemble of 10 CMIP6 Global Climate Models (e.g., MPI-ESM1-2-HR, CanESM5, and EC-EARTH3). To manage the inherent uncertainty and high model dispersion, the 50th percentile (median) of the ensemble results was selected to adjust the future design storm rainfall intensities [50]. The different baseline hyetographs with a time step resolution of 5 min are shown in Figure 5.

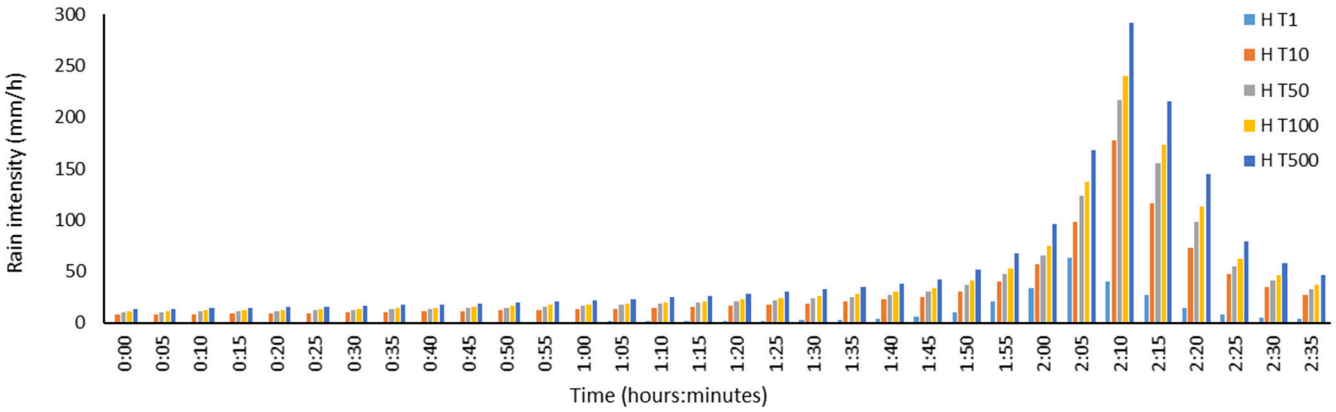

Figure 5. Hyetographs of the five baseline rainfall events, representing return periods of 1 (T1), 10 (T10), 50 (T50), 100 (T100) and 500 (T500) years [49].

2.3.2. Multi-Hazard Scenario

As for the multi-hazard scenario (MH), the following considerations were made. As part of the ICARIA project, an assessment of the joint probability of occurrence of coincident extreme precipitation and storm surges in the AMB was done based on copula models. Unfortunately, the study was inconclusive. The limited historical record of multi-hazard events in this region did not allow for a conclusive assessment of the dependence between these extreme events [56]. Nevertheless, several authors have demonstrated the frequency of this type of multi-hazard event on the coast of Catalunya [57–59]. However, none of these studies provided a joint probability assessment of these climate hazard drivers. Taking this into account, the multi-hazard scenario considers events with coincident precipitation and a storm surge in the same return period. In other words, T10 precipitation and T10 storm surge, T50 precipitation and T50 storm surge, and so on. Regarding climate variables, MH events considered the same design storms as SH simulations.

The storm surge severity was characterized with the extreme sea level (ESL) variable. This parameter represents the transient maximum sea surface elevation reached at the shoreline during coastal storm events, resulting from the combined contribution of mean sea level, storm surge, wave setup, and tidal effects [60]. In this study, ESL values were defined for the same 20 events as in the single-hazard scenario: 5 historic (T1, T10, T50, T100 and T500) and 15 climate change events based on the Shared Socio-economic Pathway 5–8.5 (five return periods per three projection periods). Such values were obtained from a detailed study of the evolution of sea level along the coast of the AMB for multiple climate change projections [60]. Table 2 collects the ESL and the maximum 5 min rain intensity of each simulation.

Table 2. Maximum 5 min intensity and extreme sea level considered in the simulations of the single-hazard and multi-hazard scenarios.

Projection Period	T1		T10		T50		T100		T500	
	$I_{5\ max}$ (mm/h)	ESL (m)	$I_{5\ max}$ (mm/h)	ESL (m)	$I_{5\ max}$ (mm/h)	ESL (m)	$I_{5\ max}$ (mm/h)	ESL (m)	$I_{5\ max}$ (mm/h)	ESL (m)
Historic	63.6	3.05	177.2	4.06	217.2	4.40	239.6	4.54	291.7	4.85
2015–2040	90.2	3.25	178.5	4.17	240.2	4.45	266.8	4.57	328.5	4.82
2041–2070	93.8	3.17	185.5	4.11	249.6	4.46	277.3	4.61	341.4	4.94
2071–2100	103.1	2.92	199.6	4.12	267.1	4.52	296.2	4.68	363.6	5.03

The ESL boundary conditions were adjusted to reflect the nature of storm surge events. ESL represented the maximum abnormal sea level reached at the shoreline, including

the effect of waves. Therefore, they were not a constant value that could be set as a fixed boundary condition. However, explicit simulation of wave behavior was beyond the scope of this study and was not suitable for a complex coupled 1D/2D model. The rapid second-scale fluctuations between wave peaks induced high variations in boundary conditions, leading to large numerical instabilities. To balance these modeling limitations while still capturing the effects of multi-hazard floods, the boundary conditions were represented by a normal distribution, with the maximum value corresponding to the peak ESL. Importantly, the peak ESL coincided with the maximum rainfall intensity, ensuring worst-case interaction between climate hazard drivers.

2.3.3. Adaptation Scenario

The climate hazard conditions considered in the adaptation scenario (AD) were the same as for the multi-hazard case (see Table 2). In terms of modeling, it was designed as a distributed hazard-mitigation strategy at the metropolitan scale, focusing on nature-based solutions and sustainable urban drainage systems that align with current local planning and infrastructure realities. As reported in previous studies in the City of Barcelona, these measures alone are insufficient to substantially reduce the risk of urban floods [61]. However, this scenario allowed us to test the sensitivity of the flood model. It included the following:

- Porous pavements: This implementation level was based on the AMB policy to prioritize permeable surfaces in specific road categories. The region has 9084 km of paved streets, of which 2930 km are designated as "Zone 30" (slow-speed single-lane streets) and 331 km host bike lanes. Applying a standard width of 1.5 m to these priority areas results in approximately 58.1 km^2 of potential implementation, which corresponds to 9% of the total street area in the metropolitan region. The realism of this measure is further supported by experimental evidence from pilots and laboratory tests at the Technical University of Catalonia, which demonstrate that these pavements can virtually eliminate runoff for the rainfall intensities simulated in this study [62,63].
- Green roofs: These have been increasingly promoted in several cities in the AMB [61]. A conservative scenario was adopted in which 10% of the 7500 public buildings in the AMB (19 km^2 in total) were assumed to be fully covered by green roofs. This assumption is aligned with the guidelines in the Barcelona Nature Plan 2030 [64,65] and the targets set by the Municipal Urban Ecology Agency. The 10% threshold is justified by local feasibility studies and the city's strategy to reach 22,000 m^2 of green roofs by 2030 [64,66,67]. In the model, these roofs are assigned an initial loss of 7 mm (up from 3 mm) and a Manning roughness of 0.4 (up from 0.015) to simulate both runoff reduction and peak flow attenuation [61,67].
- Bioretention areas: The Urban Drainage Master Plan of Barcelona identified green inner patios as strategic areas for distributed infiltration and runoff reduction [61]. A regional assessment estimated that 7.3 km^2 of these spaces could potentially be converted into bioretention areas, resulting in a 12% reduction in total effective roof area at the metropolitan scale. The dimensions and efficacy of such measures are supported by regional studies [65].

The implementation of these measures in the 1D/2D coupled model involved adjusting multiple parameters of model elements, as detailed in Table 3.

Table 3. Modeling parameters of flood adaptation measures.

Adaptation Measure	Model Element Modified	Parameter Modified	Modification Applied
Porous pavements	Subcatchments (land-use type)	Runoff contributing area	9% reduction in the effective street runoff area
Green roofs	Subcatchments (roof surface type)	Initial losses	Increased from 3 mm to 7 mm
		Manning roughness	Increased from 0.015 to 0.4
Bioretention areas	Subcatchments (roof contributing area)	Runoff contributing area	12% reduction in total roof contributing area

2.4. Impact Assessment Methods

The outputs of all 60 simulations (20 per scenario) were flood maps reflecting the maximum water depth and velocity in each cell of the model domain. The combination of these hazard maps and the impact assessment methodologies described in the following sections allowed the assessment of the socio-economic consequences of pluvial floods in the AMB.

2.4.1. Economic Impact on Buildings

This impact assessment was based on the methodology developed in Martínez-Gomáriz et al., 2021 [52], where semi-empirical depth–damage functions were developed and validated for Barcelona based on flood damage reports provided by the Spanish public insurance company. Accordingly:

- The hazard characterization for each building was based on the average flood depth in its surrounding area.
- The exposure assessment consisted of cadastral information (obtained from the Spanish Cadastre) indicating: (1) building location; (2) type of activity, classified into 14 categories; and (3) total ground floor and basement area.
- The vulnerability was characterized by the mentioned depth–damage functions, which were particularized for 14 cadastral types (see Figure 6).

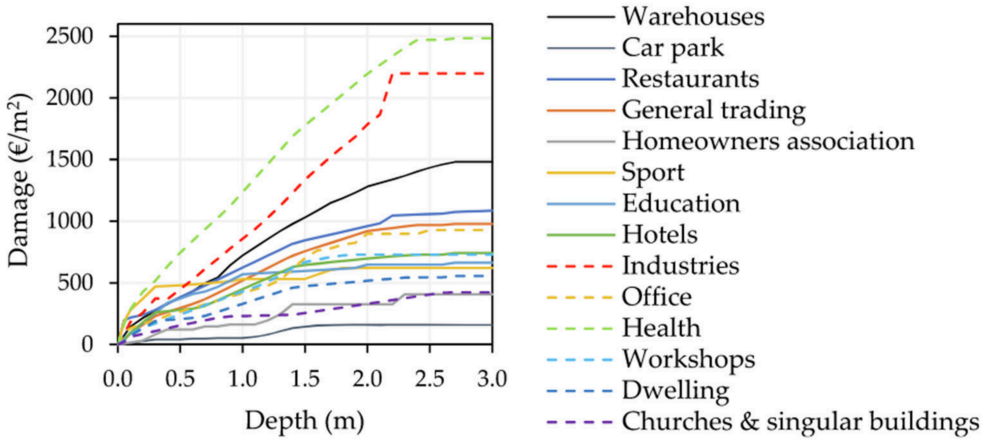

Figure 6. Depth–damage functions developed for Barcelona in year 2020 [52].

Importantly, vulnerability functions were developed based on insurance reports in the City of Barcelona until the year 2020. However, the scope of the ICARIA project went beyond this by considering 36 municipalities (including Barcelona). Correction factors were applied to the Barcelona curves to adjust the economic damage for each municipality in the AMB. This followed a methodology that considers demographic, economic, and geographic

factors influencing the cost of goods and housing repairs across Spain. Specifically, these coefficients adjusted the economic damage to the building structure and its content based on the cadastral types [52]. Table 4 presents the average correction coefficients.

Table 4. Correction factor applied to the Barcelona depth–damage curves to adjust them to the municipalities in the AMB.

Municipality	Av. Correction Coefficient	Municipality	Av. Correction Coefficient	Municipality	Av. Correction Coefficient
Badalona	0.58	El Prat de Ll.	0.42	St. Boi de Ll.	0.55
Badia de V.	0.46	Esplugues de Ll.	0.68	St. Climent de Ll.	0.42
Barberà del V.	0.56	Gavà	0.64	St. Cugat del V.	0.76
Barcelona	1.00	L'Hospitalet de Ll.	0.44	St. Feliu de Ll.	0.61
Begues	0.58	La Palma de Cervelló	0.42	St. Joan Despí	0.63
Castellbisbal	0.50	Molins de Rei	0.60	St. Just Desvern	0.74
Castelldefels	0.71	Montcada i Reixac	0.55	St. Vicenç dels Horts	0.52
Cerdanyola del V.	0.58	Montgat	0.60	Sta. Coloma de C.	0.42
Cervelló	0.51	Pallejà	0.53	Sta. Coloma de G.	0.52
Corbera de Ll.	0.50	Ripollet	0.54	Tiana	0.64
Cornellà de Ll.	0.57	Sant Adrià de B.	0.42	Torrelles de Ll.	0.51
El Papiol	0.43	St. Andreu de la B.	0.54	Viladecans	0.56

2.4.2. Risk Assessment for Pedestrians

Following the criteria in Russo et al., 2013 [68], flood hazard classification for pedestrians was based on the combination of maximum water depth and velocity reached in the 2D domain of the model. Therefore, each cell of the flood maps was characterized as "low", "medium", or "high" hazard according to Figure 7a.

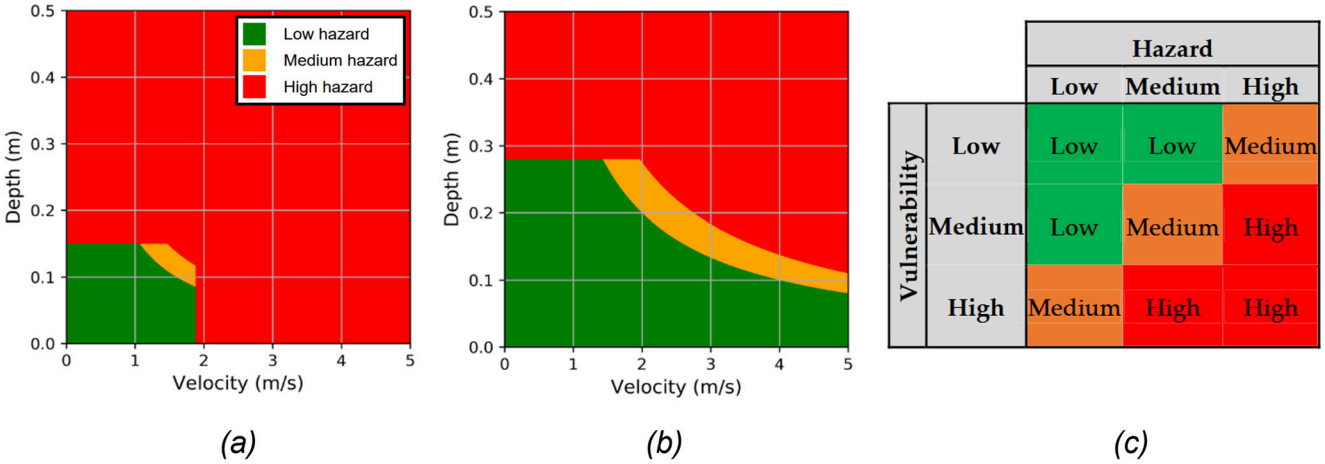

Figure 7. Criteria for (**a**) pedestrian hazard classification, (**b**) vehicle hazard classification, and (**c**) risk classification matrix [26].

In this case, the exposure and vulnerability assessments depended on demographic data of all census tracts (in Spanish, "secciones censales"). Each one was classified based on thresholds proposed in [26]: percentage of population above 65 years old, percentage of

foreign inhabitants, and population density. Accordingly, the vulnerability of each census tract was classified as "low", "medium", or "high".

The risk characterization for pedestrians was based on the risk matrix overlapping the hazard classification and the vulnerability assessment (Figure 7c). In other words, each mesh element in the model domain received a risk classification according to its hazard level and the vulnerability level of its corresponding census tract.

2.4.3. Risk Assessment on Vehicles

Similar to the previous section, Martínez-Gomáriz et al., 2017 [26], defined thresholds to assess the stability of vehicles exposed to floods (see Figure 7b). The exposure assessment considered the whole road network of the flood model domain. The vulnerability of each section was defined based on its importance category as is defined in OpenStreet maps. According to this, all highways, roads, and primary and secondary links were classified as "high" vulnerability, tertiary links as "medium" vulnerability, and residential streets as "low" vulnerability. Other studies could adjust this classification with vehicular intensity data from the area of study [26]. However, this information was not homogeneously available for the AMB. The risk assigned to each road section considered the same matrix as for pedestrians (Figure 7c).

2.5. Scenario Comparison

The comparison between the 60 scenarios was based on risk indicators. Risk for buildings was quantified in terms of economic damage (€), risk for pedestrians was expressed through high-risk areas (ha), and risk for vehicles was evaluated through the length of high-risk road segments (km). This allowed a standardized comparison of scenarios. Variations in the flood hazard maps, which are reflected in the spatial extent of flooding, water depth, and flow velocity, were not explicitly assessed.

3. Results

3.1. Economic Impact on Buildings Resutls

The comparison of scenarios in Table 5 shows three clear and consistent patterns for flood-related economic damage to properties. First, climate change increases absolute losses across all return periods, particularly toward the end of the century (Period 3, 2071–2100). Even under the SH configuration, damages rise steadily; for example, T10 losses increase from 217 M€ (historic) to 294 M€ (2071–2100), and T500 losses from 1244 M€ to 1451 M€. Second, the transition from single-hazard (SH) to multi-hazard (MH) conditions generates additional impacts in almost all cases, generally around +4% to +7% for T10–T100 events, reaching up to +15% in some T500 projections. Since the SH baseline T1 simulation shows very limited damage, a comparatively large increase appears in the MH case. In future periods, however, T1 simulations stabilize to differences of approximately +4–9%. Third, the adaptation (AD) scenario demonstrates a clear capacity to reduce damages across all simulations. For moderate events (T10), damage reductions range between −14% and −18%; for T50, between −11% and −15%; and for T100, around −9% to −11%. Even for extreme events (T500), reductions remain significant, generally between −7% and −10%. The largest relative benefits are observed for more frequent events (T1 and T10) rather than for extreme cases. This pattern is consistent with the type of measures implemented, many of which are nature-based solutions. By definition, these urban elements are more appropriate to reduce runoff for low return periods (e.g., T1 to T10), while their effectiveness becomes more limited under higher-magnitude events.

Table 5. Economic damage to properties for all flood simulations.

Economic Damage to Properties per Return Period and Projection Periods (Percentage of Change When Comparing SH to MH and MH to AD Scenarios)			
T1			
Projection Period	**SH Scenario**	**MH Scenario**	**AD Scenario**
Historic	0.01 M€	0.15 M€ (>100%)	0.13 M€ (−10%)
Period 1 (2015–2040)	4.4 M€	4.8 M€ (+9%)	4.0 M€ (−16%)
Period 2 (2041–2070)	4.8 M€	5.2 M€ (+8%)	4.2 M€ (−20%)
Period 3 (2071–2100)	7.8 M€	8.1 M€ (+4%)	6.6 M€ (−19%)
T10			
Projection Period	**SH scenario**	**MH scenario**	**AD scenario**
Historic	217.4 M€	226.4 M€ (+4%)	185.5 M€ (−18%)
Period 1 (2015–2040)	252.2 M€	264 M€ (+5%)	221.0 M€ (−16%)
Period 2 (2041–2070)	267.8 M€	279.6 M€ (+4%)	239.6 M€ (−14%)
Period 3 (2071–2100)	293.8 M€	306.9 M€ (+4%)	254.1 M€ (−17%)
T50			
Projection Period	**SH scenario**	**MH scenario**	**AD scenario**
Historic	493 M€	516.9 M€ (+5%)	438.4 M€ (−15%)
Period 1 (2015–2040)	551.3 M€	579.8 M€ (+5%)	514.4 M€ (−11%)
Period 2 (2041–2070)	565.4 M€	603.3 M€ (+7%)	529.6 M€ (−12%)
Period 3 (2071–2100)	648.7 M€	683.4 M€ (+5%)	606.7 M€ (−11%)
T100			
Projection Period	**SH scenario**	**MH scenario**	**AD scenario**
Historic	685.1 M€	717.1 M€ (+5%)	653.5 M€ (−9%)
Period 1 (2015–2040)	750.3 M€	785.8 M€ (+5%)	703.9 M€ (−10%)
Period 2 (2041–2070)	767 M€	809.5 M€ (+6%)	716.8 M€ (−11%)
Period 3 (2071–2100)	876.5 M€	919.8 M€ (+5%)	821.7 M€ (−11%)
T500			
Projection Period	**SH scenario**	**MH scenario**	**AD scenario**
Historic	1244.2 M€	1290.5 M€ (+4%)	1155.8 M€ (−10%)
Period 1 (2015–2040)	1319.7 M€	1371.5 M€ (+15%)	1245.9 M€ (−9%)
Period 2 (2041–2070)	1344.9 M€	1412.9 M€ (+5%)	1271.3 M€ (−10%)
Period 3 (2071–2100)	1451.3 M€	1538.8 M€ (+6%)	1428.7 M€ (−7%)

Figure 8 reflects the economic damage distribution among the 36 municipalities in the AMB for the SH scenario simulations. Barcelona is the most affected municipality, with damages up to 53 M€ for a T10 SH event. This could rise to 81.5 M€ by the end of the century. Other important municipalities, such as Badalona, Castelldefels, Montcada i Reixac, St. Boi de Llobregat, St. Cugat del Vallès and Viladecans, could suffer economic damages exceeding 10 M€. Logically, these municipalities correspond to the most extensively damaged ones, with a higher number of assets exposed. Smaller municipalities accumulate fewer losses regardless of their location in the region (coastal or inland).

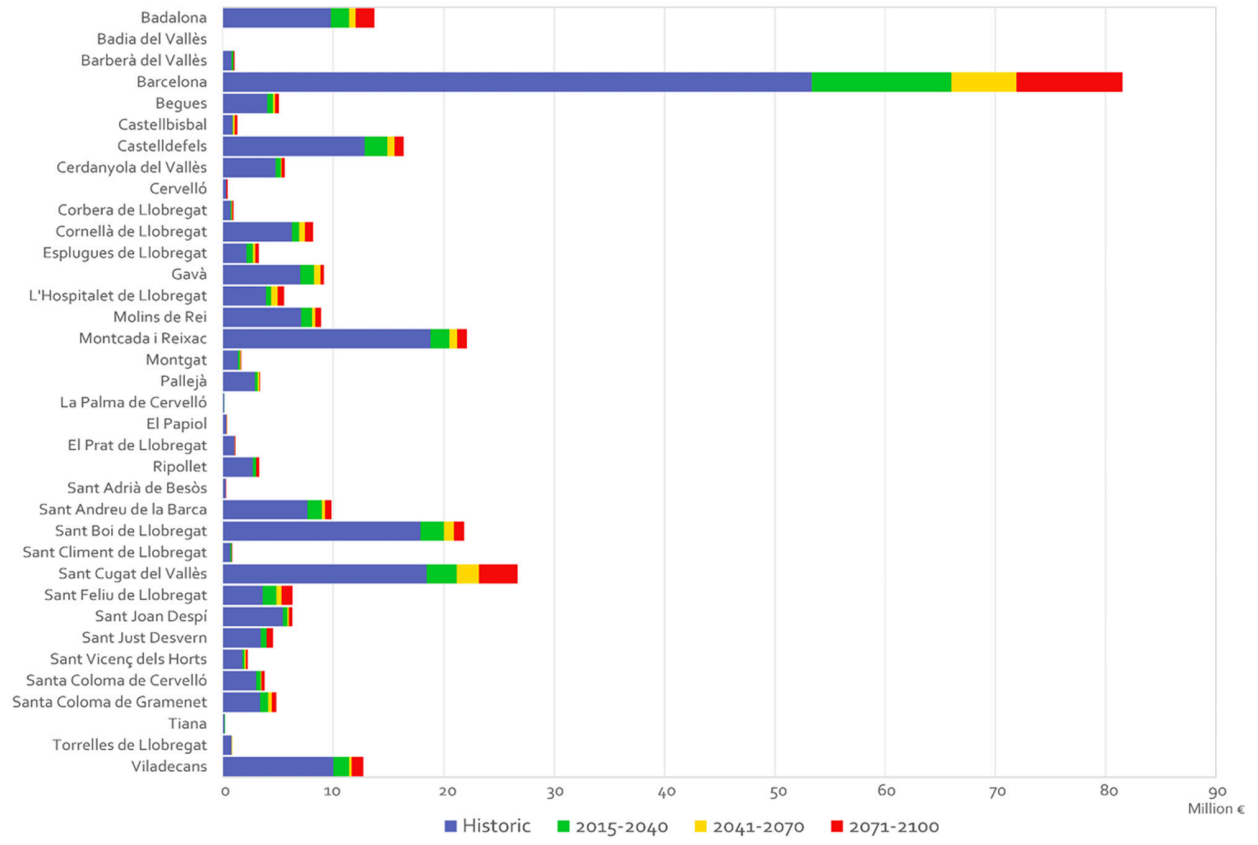

Figure 8. Economic damage distribution among the municipalities in the AMB (T10 event SH scenario). Source: Authors.

Besides the total economic damage associated with each simulation, the expected annual damage (EAD) provides a more balanced view of the potential impacts of floods. The EAD is a probabilistic indicator that represents the long-term average economic loss caused by flooding over one year [69]. Rather than describing the damage from a single event (e.g., a 10-year or 100-year storm), the EAD integrates damage from multiple flood events of different magnitudes, each weighted by its probability of occurrence. Mathematically, it corresponds to the area under the curve that relates flood damage to event probability (see Figure 9). In this way, both frequent, low-impact events and rare, high-impact events contribute to the final value.

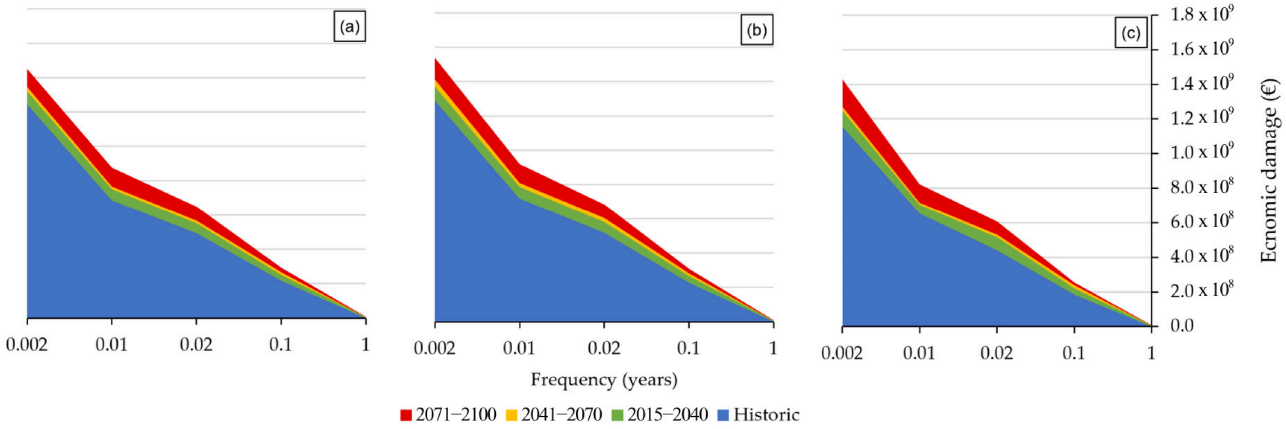

Figure 9. Damage–probability curve for the three scenarios: (**a**) SH, (**b**) MH, and (**c**) AD. Source: Authors.

Table 6 shows a progressive increase in the EAD across all scenarios and projection periods. Comparing the historic baseline and Period 3 (2071–2100) results, the EAD increases from 139.8 M€ to 190.3 M€ in the SH scenario (+36.1%) and from 145.9 M€ to 199.2 M€ in the MH scenario (+36.5%). The increase in both scenarios is virtually the same, but MH yields more damage due to the larger floods in coastal areas. The damage gap remains nearly constant, with absolute differences between 6 M€ and 9 M€.

Table 6. EAD for all scenarios and projection periods.

Projection Period	EAD SH Scenario	EAD MH Scenario	EAD AD Scenario
Historic	139.8 M€	145.9 M€	121.2 M€
Period 1 (2015–2040)	162.3 M€	170.2 M€	144.6 M€
Period 2 (2041–2070)	171.1 M€	179.4 M€	154.7 M€
Period 3 (2071–2100)	190.3 M€	199.2 M€	167.9 M€

3.2. Risk for Pedestrians Resutls

The evolution of the total high-risk area for pedestrians shows similar patterns to those observed for economic damage to properties. High-risk areas increase progressively across all return periods toward the end of the century, with a higher risk in the MH scenario compared to the SH scenario and a lower risk in the AD simulations with respect to the MH scenario (see Table 7).

Under the SH hypothesis, T10 high-risk surfaces expand from approximately 494 ha (historic) to 621 ha (2071–2100), while T100 areas grow from 1175 ha to 1401 ha. The MH scenario produces a general increase in high-risk areas between +3% and +6% for T10–T100 events and up to +8% for T50 in some mid-century projections. In contrast, for T500 events, the difference between SH and MH scenarios is marginal (0–4%). This supports the idea that for very extreme rainfall, the pluvial component dominates the hazard conditions and limits the relative influence of sea-level boundary conditions. The AD scenario consistently reduces the spatial extent of high-risk areas compared to the multi-hazard baseline, with reductions generally ranging from −8% to −12% for T10 to T100 events and reaching up to −17% to −19% for T1 in future periods. For T100, they remain around −7% to −9%. Even under extreme T500 conditions, adaptation achieves a significant reduction (−6% to −7%) except in the end-of-century simulation (Period 3, 2071–2100), where the risk reduction is null.

Regarding the spatial distribution of pedestrian risk in Figure 10, a clear pattern is observed. Most peri-urban streams are classified as medium-risk areas, as they concentrate high water depths and velocities and are located in low- to non-populated areas with low exposure and low vulnerability. High-risk areas are found in either steep terrain or low-lying urban areas. Despite accumulating less water than peri-urban streams, their location in densely populated areas raises the local vulnerability index. When comparing the same return periods across different climate change projections, it can be seen that future high-risk areas tend to extend around the ones already identified for the historic scenario. Comparing T10 to T500 simulations, the extent of medium-risk areas grows around the peri-urban streams, while it remains stable in the fluvial and coastal plains. High-risk areas mainly increase in the urban areas, particularly around areas already identified as high-risk in the T10 map.

More detailed maps are shown in Figure 11. High-risk areas are concentrated in densely populated zones such as Castelldefels and the Poblenou neighborhood (Barcelona). In Poblenou, under the SH scenario (Figure 11a), risk is mainly concentrated in the lower-central part of the domain, while in the MH scenario (Figure 11b), risk expands around these already affected areas, illustrating the growth of high-risk spaces particularly in coastal

zones under storm surge conditions. In Castelldefels, the situation is similar: differences between the SH (Figure 11c) and MH (Figure 11d) scenarios are mainly found in coastal neighborhoods, where the influence of sea level effectively affects the performance of the sewer system. Overall, differences between scenarios remain spatially consistent, with the MH scenario primarily intensifying existing hotspots rather than significantly expanding the total extent of risk.

Table 7. High-risk area for pedestrians for all flood simulations.

High-Risk Area for Pedestrians (ha) per Return Period and Projection Periods (Percentage of Change When Comparing SH to MH and MH to AD Scenarios)			
T1			
Projection Period	**SH Scenario**	**MH Scenario**	**AD Scenario**
Historic	0.00	1.69 (>100%)	1.68 (−1%)
Period 1 (2015–2040)	19.42	22.73 (+17%)	18.76 (−17%)
Period 2 (2041–2070)	20.94	23.99 (+15%)	20.22 (−16%)
Period 3 (2071–2100)	31.54	34.2 (+8%)	27.86 (−19%)
T10			
Projection Period	**SH scenario**	**MH scenario**	**AD scenario**
Historic	494.14	513.02 (+4%)	449.67 (−12%)
Period 1 (2015–2040)	554.06	579.34 (+5%)	516.88 (−11%)
Period 2 (2041–2070)	577.69	601.15 (+4%)	543.37 (−10%)
Period 3 (2071–2100)	620.75	647.06 (+4%)	575.15 (−11%)
T50			
Projection Period	**SH scenario**	**MH scenario**	**AD scenario**
Historic	918.68	952.08 (+4%)	858.99 (−10%)
Period 1 (2015–2040)	987.67	1042.69 (+6%)	958.47 (−8%)
Period 2 (2041–2070)	1007.35	1085.16 (+8%)	978.5 (−10%)
Period 3 (2071–2100)	1121.02	1185.93 (+6%)	1083.58 (−9%)
T100			
Projection Period	**SH scenario**	**MH scenario**	**AD scenario**
Historic	1174.76	1208.21 (+3%)	1125.2 (−7%)
Period 1 (2015–2040)	1245.11	1299.32 (+4%)	1198.65 (−8%)
Period 2 (2041–2070)	1270.60	1333.94 (+5%)	1214.66 (−9%)
Period 3 (2071–2100)	1400.63	1463.34 (+4%)	1347.11 (−8%)
T500			
Projection Period	**SH scenario**	**MH scenario**	**AD scenario**
Historic	1818.69	1798.78 (0%)	1686.98 (−6%)
Period 1 (2015–2040)	1856.01	1916.64 (+3%)	1782.63 (−7%)
Period 2 (2041–2070)	1879.70	1955.57 (+4%)	1809.08 (−7%)
Period 3 (2071–2100)	1972.91	1956.82 (0%)	1956.74 (0%)

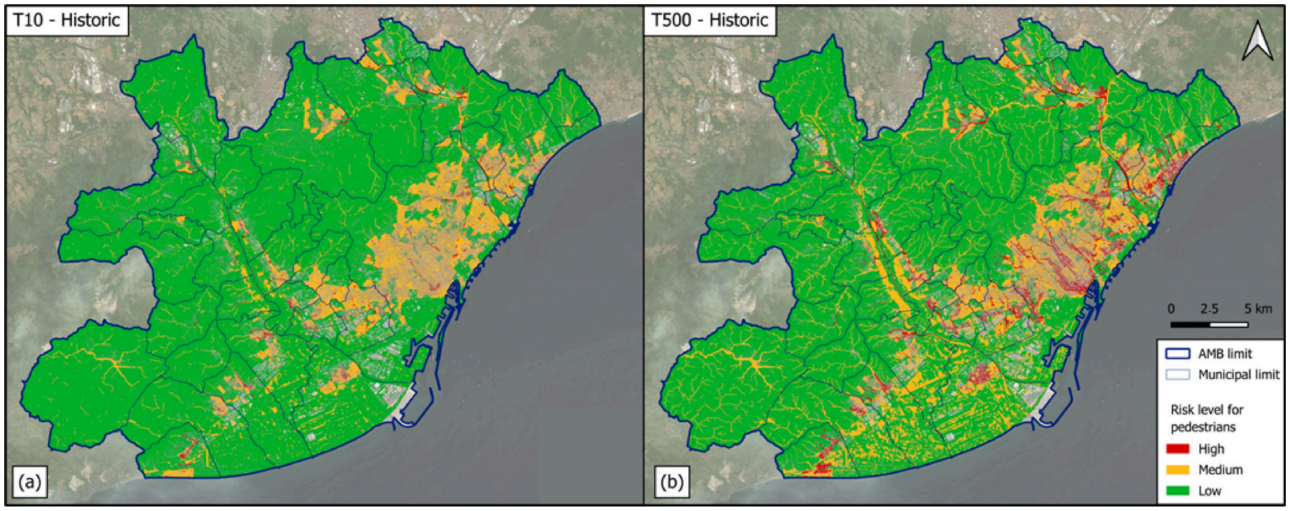

Figure 10. Map of pedestrian risk for: (**a**) T10 historic SH, and (**b**) T500 historic SH events. Source: Authors.

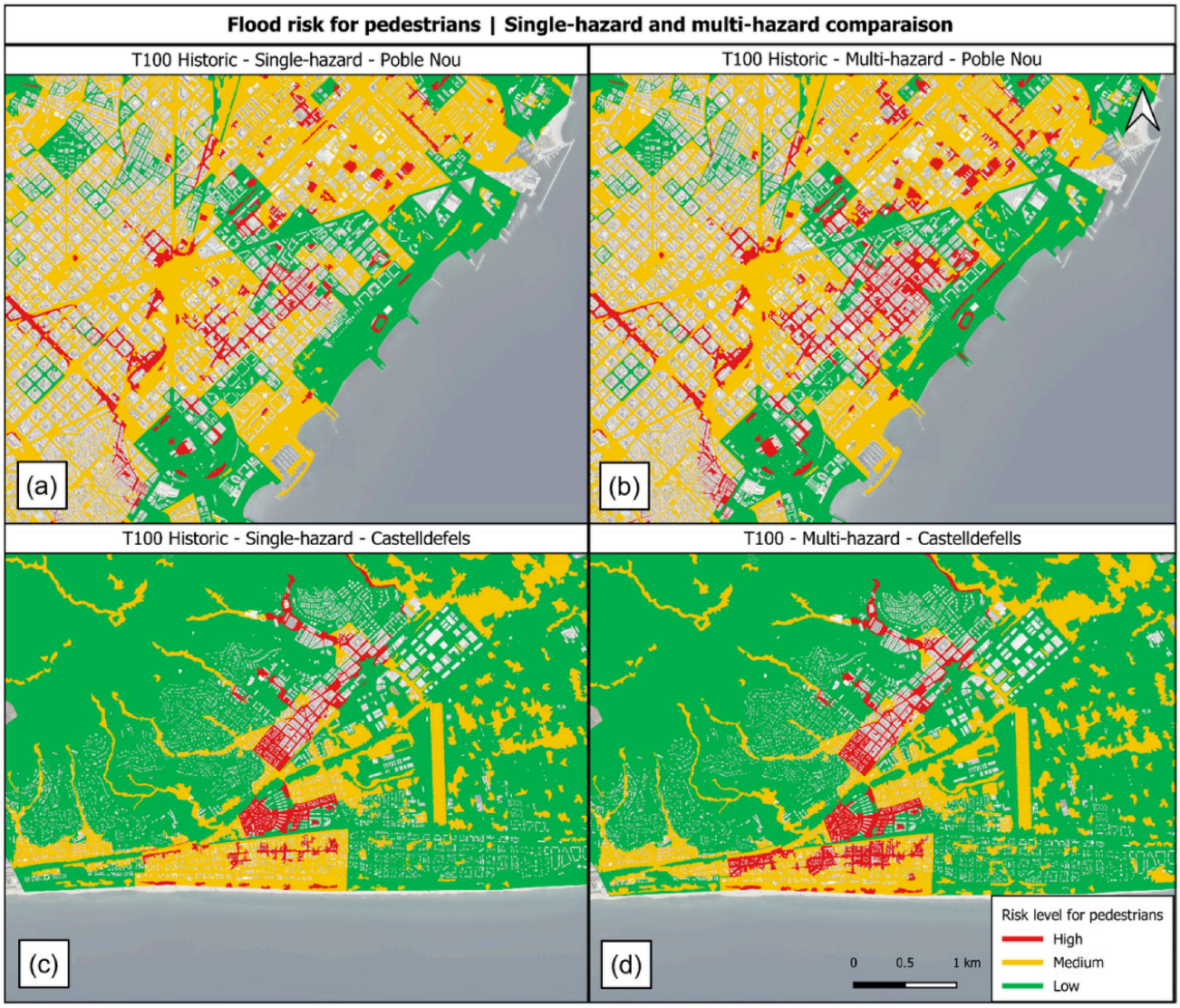

Figure 11. Detailed maps of risk areas for pedestrians for T100 historic events corresponding to (**a**) SH scenario in the Poblenou neighborhood (Barcelona), (**b**) MH scenario in the Poblenou neighborhood (Barcelona), (**c**) SH scenario in Castelldefels, and (**d**) MH scenario in Castelldefels. Source: Authors.

3.3. Risk to Vehicles Resutls

The assessment of high-risk road segments for vehicles confirms the same trends as in the previous sections. Climate change, and in particular multi-hazard events, increase the risk to traffic in the AMB (see Table 8).

Table 8. High-risk roads for vehicles for all flood simulations.

High-Risk Roads for Vehicles (km) per Return Period and Projection Periods (Percentage of Change When Comparing SH to MH and MH to AD Scenarios)			
T1			
Projection Period	**SH Scenario**	**MH Scenario**	**AD Scenario**
Historic	0.09	0.08 (0%)	0.08 (0%)
2015–2040	3.64	3.84 (+5%)	3.37 (−12%)
2041–2070	3.66	3.91 (+7%)	3.65 (−7%)
2071–2100	5.01	4.95 (0%)	4.48 (−9%)
T10			
Projection Period	**SH scenario**	**MH scenario**	**AD scenario**
Historic	59.11	59.05 (0%)	53.73 (−9%)
Period 1 (2015–2040)	65.32	66.7 (+2%)	60.97 (−9%)
Period 2 (2041–2070)	69.37	70.42 (+2%)	64.71 (−8%)
Period 3 (2071–2100)	74.37	75.79 (+2%)	68.81 (−9%)
T50			
Projection Period	**SH scenario**	**MH scenario**	**AD scenario**
Historic	120.54	124.28 (+3%)	109.23 (−12%)
Period 1 (2015–2040)	132.45	137.41 (+4%)	123.07 (−10%)
Period 2 (2041–2070)	135.54	142.53 (+5%)	127.73 (−10%)
Period 3 (2071–2100)	151.54	159 (+5%)	145.83 (−8%)
T100			
Projection Period	**SH scenario**	**MH scenario**	**AD scenario**
Historic	160.17	163.88 (+2%)	153.76 (−6%)
Period 1 (2015–2040)	172.55	177.45 (+3%)	165.58 (−7%)
Period 2 (2041–2070)	175.47	183.57 (+5%)	168.13 (−8%)
Period 3 (2071–2100)	198.88	207.18 (+4%)	187.27 (−10%)
T500			
Projection Period	**SH scenario**	**MH scenario**	**AD scenario**
Historic	271.26	274.77 (+1%)	252.23 (−8%)
Period 1 (2015–2040)	282.11	294.77 (+4%)	268.84 (−9%)
Period 2 (2041–2070)	287.24	301.79 (+5%)	274.4 (−9%)
Period 3 (2071–2100)	306.55	308.3 (+1%)	304.36 (−1%)

The SH simulations show that the total length of roads classified as high-risk increases for all return periods. For instance, T10 segments rise from about 59 km (historic) to 74 km (late-century), and T100 from 160 km to nearly 199 km. Extreme events (T500) show a similar trajectory, reaching more than 306 km by the end of the century. When MH conditions are introduced, the increase in high-risk road extent is positive but limited, typically between

+2% and +8% for T10 to T100 simulations. For some T500 cases, differences are negligible (0–1%), indicating that coastal backwater effects influence the specific low-lying stretches rather than the whole extent of the metropolitan area. Overall, compound (multi-hazard) flooding slightly aggravates network vulnerability, particularly in coastal municipalities, but does not radically change the metropolitan-scale totals. The AD scenario achieves consistent reductions in the extent of high-risk road segments of between 6 and 12% across all simulations. Even for T500 events, adaptation reduces risk by roughly 8% except for the long-term projection period, where the reduction is not significant.

The distribution of risk for vehicles in Figure 12 reflects that most highways and inter-urban roads are classified as medium-risk areas even for T10 events. Despite the fact that such infrastructure is built with measures to prevent flooding, their high traffic intensity makes them particularly vulnerable parts of the transport network. High-risk areas for vehicles are concentrated in the flood-prone urban areas, following a similar distribution to that of high-risk areas for pedestrians (Figure 10). These streets combine high hazard conditions (elevated water depth and velocities) with high traffic intensity, causing high vulnerability classification.

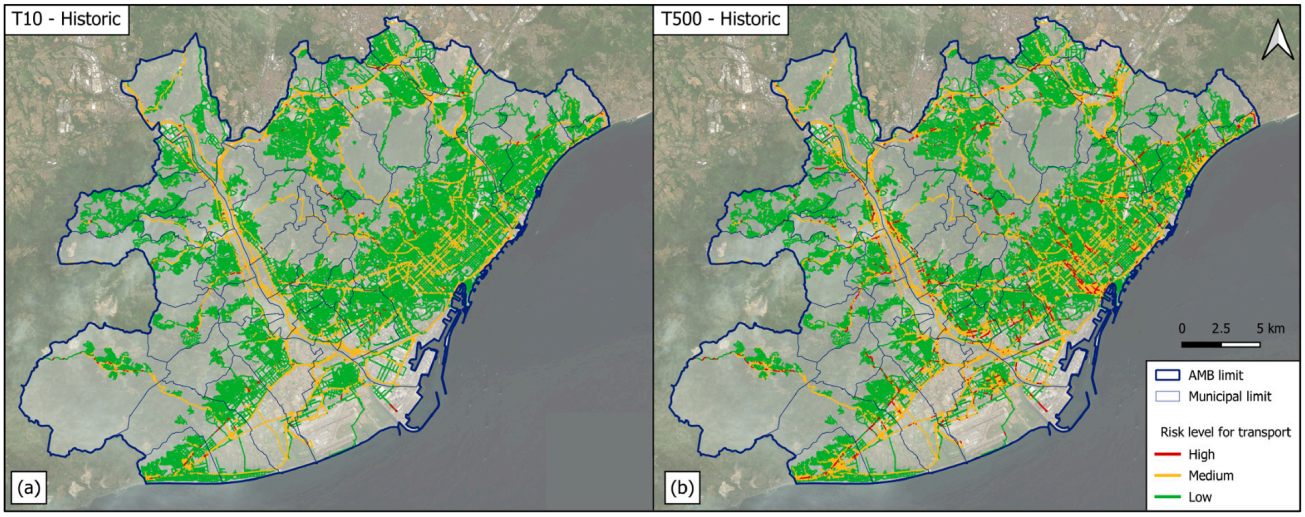

Figure 12. Maps of vehicle risk for: (**a**) T10 historic SH and (**b**) T500 historic SH events. Source: Authors.

Figure 13 compares the growth of vehicle-related risk in the historic T100 event under SH and MH conditions. In the Poblenou neighborhood of Barcelona, high-risk road segments increase substantially under the MH scenario (Figure 13b), with a clearer continuity of affected links expanding from the main hotspots identified in SH conditions (Figure 13a). In Castelldefels, high-risk segments remain relatively stable between scenarios, while medium-risk road segments expand notably along the coastal area, reflecting the influence of sea-level conditions on network performance (Figure 13c,d).

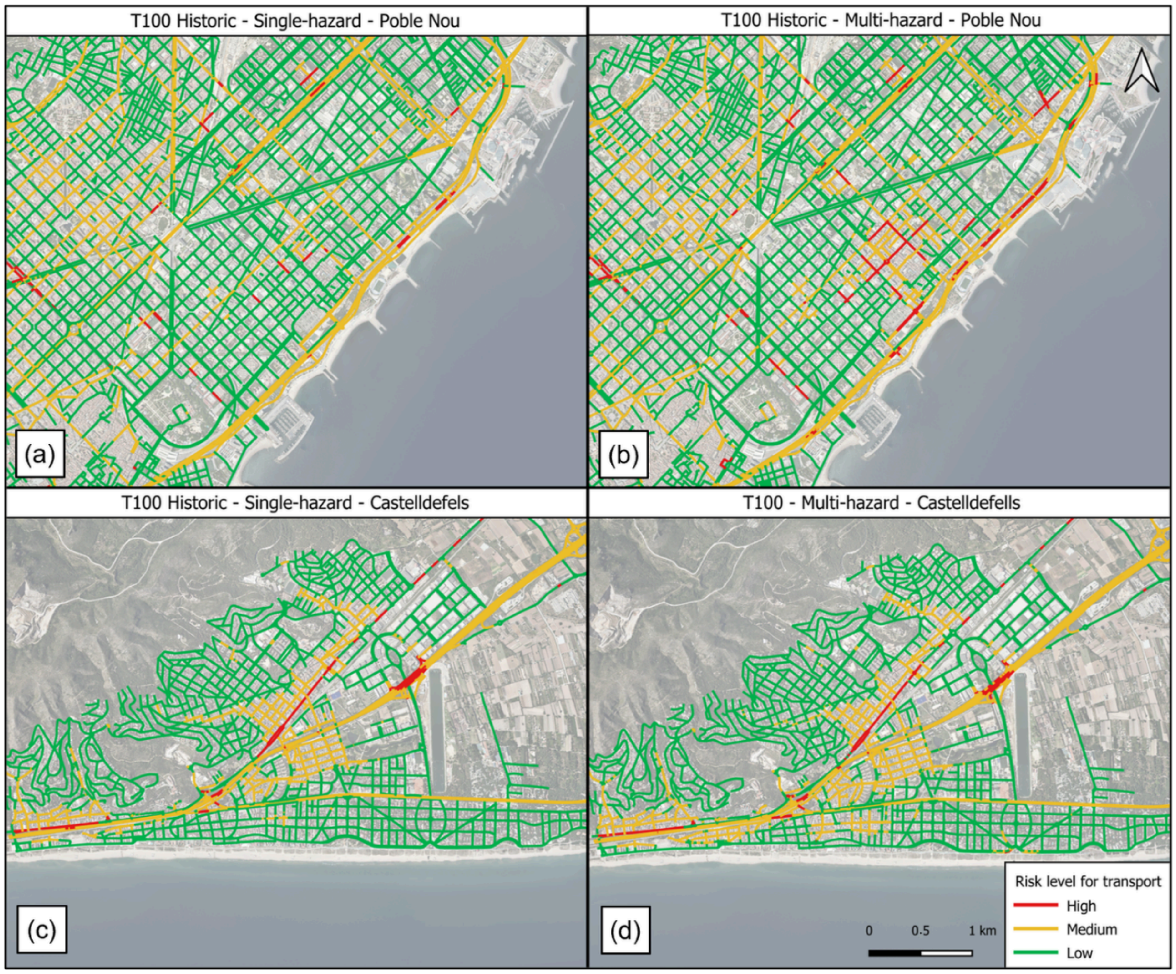

Figure 13. Detailed maps of risk areas for vehicles for the T100 historic events corresponding to (**a**) SH scenario in the Poblenou neighborhood (Barcelona), (**b**) MH scenario in the Poblenou neighborhood (Barcelona), (**c**) SH scenario in Castelldefels, and (**d**) MH scenario in Castelldefels. Source: Authors.

4. Discussion

The socio-economic impacts of floods were already studied in Barcelona in the RESCCUE project using similar methods [25]. Importantly, the RESCCUE economic damage results were validated by comparing real flood event simulations with the corresponding insurance reports for the same dates [52].

The ICARIA and RESCCUE projects considered the same historic rain events. However, the long-term projections differed: the first considered Shared Socio-economic Pathway 5–8.5, while the latter used Representative Concentration Pathway 8.5. For both, the projection period was 2071 to 2100. Such information is a valuable reference when discussing the results presented in the ICARIA project.

The comparison of direct economic damages to buildings in Barcelona derived from the ICARIA and RESCCUE projects (Figure 14) shows a generally consistent pattern. However, ICARIA estimated higher damages for both historic and future simulations. Although both projects used the same historic rainfall events, they employed different 1D/2D hydrodynamic models, in particular regarding the runoff routing to the sewer system. ICARIA's model was "hybrid": rainfall was directly applied to the mesh and 2D runoff computed until it entered the sewer system. On the contrary, the RESCCUE and PDSIBA approaches conveyed all runoff to the sewer network, and only the water reaching the surface from pressurized pipes was computed in the 2D domain. Such differences affect the final results.

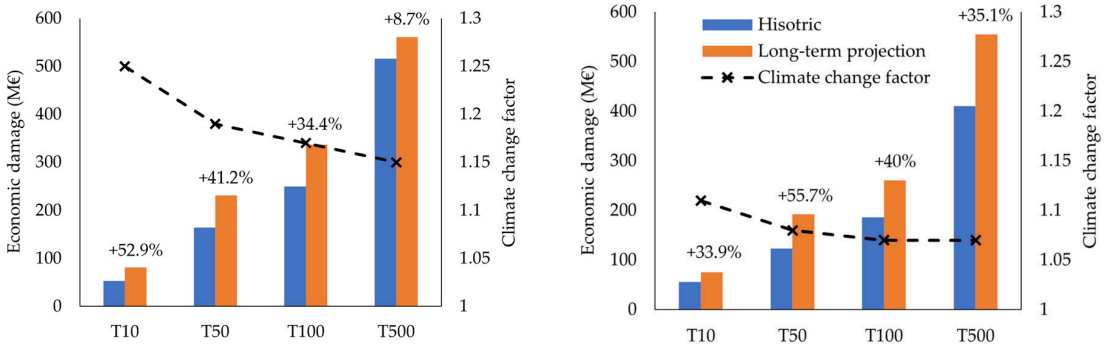

	ICARIA				RESCCUE			
Return period	**T10**	**T50**	**T100**	**T500**	**T10**	**T50**	**T100**	**T500**
Historic damage (M€)	53.3	164.2	250.5	516.5	56.4	123.6	186.3	410.9
Long-term damage (M€)	81.5	231.9	336.6	561.3	75.5	192.5	260.8	555.3
Climate change factor	1.25	1.19	1.17	1.15	1.11	1.08	1.07	1.07

Figure 14. Results of the economic impact of properties in Barcelona for projects ICARIA and RESCCUE [25].

Despite these methodological differences, both datasets show a similar overall trend in the growing evolution of damages between historic conditions and climate change projections for the same return periods. The relative increase in damages varies depending on the return period. For the most extreme events (T50, T100, and T500), the percentage increase in damages estimated by RESCCUE is 15% to 27% higher than that obtained by ICARIA.

The most significant difference is the T500 event under future climate conditions. ICARIA estimates an increase in damages of 8.5% relative to the historic scenario, whereas RESCCUE projects a 35.5% increase. Two main factors can explain this discrepancy. First, very rare events such as the T500 rainfall scenario are associated with greater uncertainty, as climate models show substantial dispersion for these cases. Second, the two projects applied different climate change factors resulting from different climate change scenarios. RESCCUE considered climate change factors of 7 to 15%, while ICARIA's were 15 to 25%. This difference is very substantial and has a direct effect on the potential flood impacts since, according to its design criteria, a T10 historic event saturates Barcelona's sewer network. Therefore, growing climate change coefficients generate more runoff that cannot be conveyed by the drainage system, resulting in more water accumulation in the streets capable of damaging assets.

Results in Figure 15 show a similar evolution of high-risk areas for pedestrians in both datasets. For the lower return periods (T10 and T50), RESCCUE estimates larger risks for both the historic and the future simulations, while ICARIA does so for the extreme events (T100 and T500). Except for T10, RESCCUE projects larger risk increases within each return period despite considering smaller climate change factors. As discussed previously, variations in the 1D/2D flood models can lead to different flood depth and velocity distributions, which directly affect the spatial extent of areas classified as hazardous for pedestrians. Remarkably, the evolution of pedestrian risk across return periods resembles the trends observed for direct economic damages to properties. In both cases, the two modeling frameworks produce comparable patterns despite differences in magnitude.

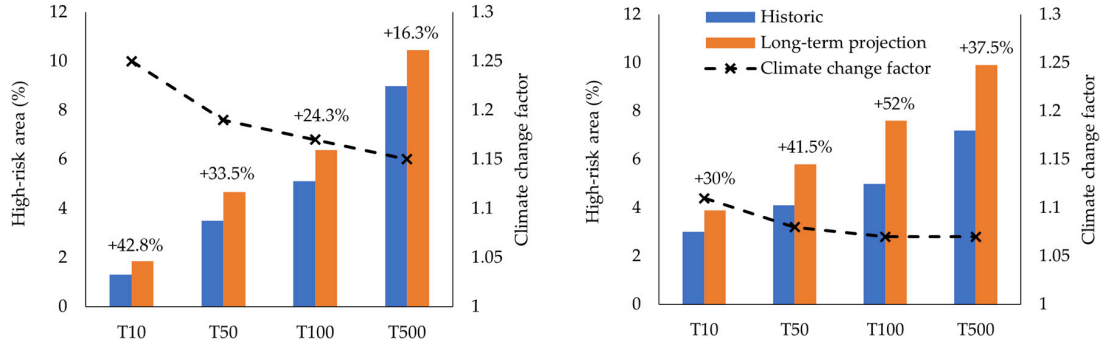

	ICARIA				RESCCUE			
Return period	**T10**	**T50**	**T100**	**T500**	**T10**	**T50**	**T100**	**T500**
Historic high-risk area (%)	1.3	3.5	5.1	9.0	3.0	4.1	5.0	7.2
Long-term high-risk area (%)	1.9	4.7	6.4	10.5	3.9	5.8	7.6	9.9
Climate change factor	1.25	1.19	1.17	1.15	1.11	1.08	1.07	1.07

Figure 15. Results of high-risk area for pedestrians in Barcelona for ICARIA and RESCCUE projects [25].

Figure 16 compares the EAD and the EAD per capita (single-hazard scenario) of all municipalities in the AMB based on ICARIA's results. In this figure, the municipalities are ordered according to their population. Several ideas can be extracted from this. Firstly, Barcelona stands as an outlier in the EAD scale. Given that it is the largest municipality and has the largest concentration of buildings, logically, it accumulates the majority of the economic damage. However, its EAD per capita is among the lowest. On the one hand, its large population reduces this ratio. On the other hand, this city has a well-prepared sewer network, equipped with several anti-flood storage facilities and multiple adaptation measures that mitigate the impact of floods [25].

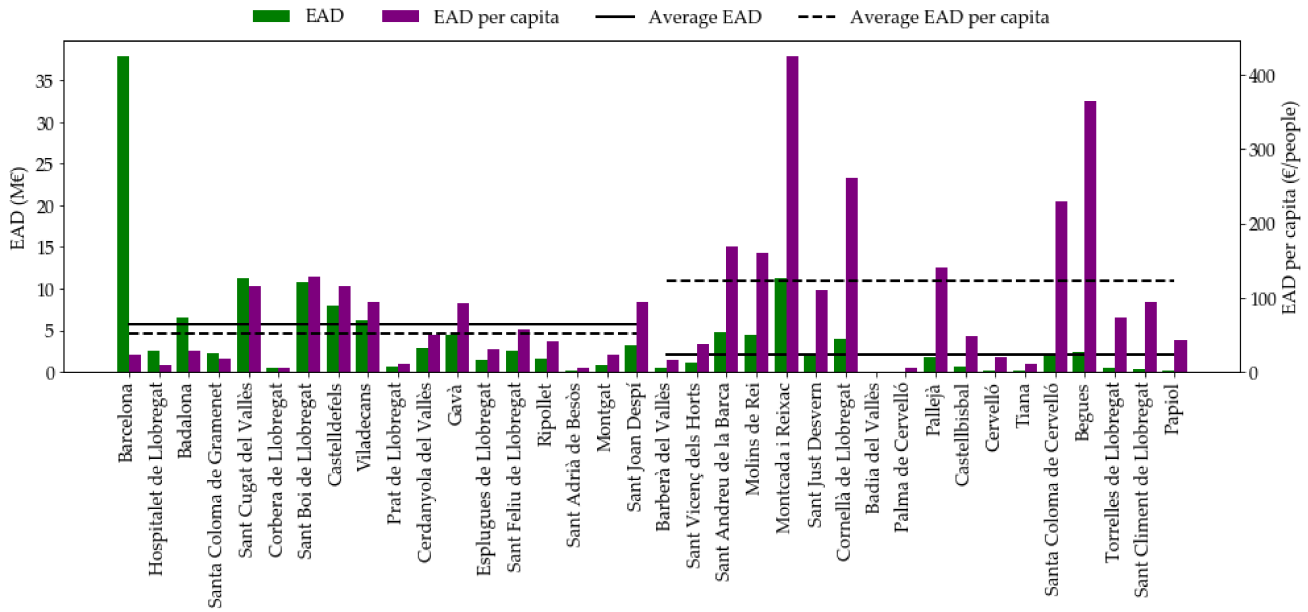

Figure 16. Comparison of EAD and EAD per capita for each municipality of the AMB (ordered by number of inhabitants) based on ICARIA's results of economic impact on properties.

Secondly, the 18 most populated municipalities have a mean EAD of 5.7 M€, while the 18 least inhabited report 2 M€. As for the EAD per capita, the values are 52 and 234 €/person, respectively. Thirdly, it can be observed that some municipalities in the second group (e.g., Montcada i Reixac, Cornellà de Llobregat and Begues) have a very high EAD per capita, while their total EAD is within the same range as similar cases.

This information highlights that investing in flood resilience in municipalities with a low total EAD but a high EAD per capita may have a limited impact on overall metropolitan-scale damage yet can offer substantial local cost benefits. Conversely, implementing flood protection measures in municipalities with a higher total EAD can significantly reduce the bulk of flood-related economic damages across the region.

This study acknowledges several limitations to be considered when interpreting the results. Firstly, the multi-hazard events are based on a simplified assumption. A deeper understanding of the correlation between coincident precipitation and storm surge events would support a more realistic definition of events. Second, the model calibration is based on a reduced dataset of field measurements given the extent of the model. Third, this methodology aggregates heterogeneous datasets, including sewer network information, terrain data, and socio-economic indicators, whose availability and quality may vary across the 36 municipalities. Fourth, the influence of SSP scenarios is limited to the modification of rainfall patterns, while potential changes in socio-economic, demographic, and urban development conditions within the AMB are not considered. Future work should apply or develop methodologies to improve these aspects and reduce their associated uncertainty.

5. Conclusions

This study provides a comprehensive assessment of the socio-economic impacts of pluvial and compound (multi-hazard) floods in the Metropolitan Area of Barcelona (AMB) under current and future climate conditions, as part of the ICARIA project. To achieve this, a large-scale coupled 1D/2D hydrodynamic model was developed, integrating the complex underground drainage systems of 36 municipalities with surface runoff dynamics.

This study goes beyond previous research by applying high-resolution coupled 1D/2D hydrodynamic models at the regional scale while maintaining detailed sewer network representation, integrating socio-economically tailored vulnerability curves, incorporating updated climate change projections, and adopting a multi-hazard approach.

The methodology involved simulating 60 distinct events across three scenarios, single-hazard (SH), multi-hazard (MH), and adaptation (AD), considering historic and future climate change projections. Results indicate a significant upward trend in flood-related impacts. In the SH scenario, the EAD in the AMB is projected to increase by 36.1%, rising from 139.8 M€ to 190.3 M€ by the end of the century. When considering multi-hazard conditions, the EAD reaches 199.2 M€, representing a 36.5% increase and highlighting the additional vulnerability of coastal areas to backwater effects. Furthermore, the spatial extent of high-risk zones expands considerably; for instance, high-risk areas for pedestrians in a 10-year return period event are expected to grow from 494 ha to 621 ha, while high-risk road segments for vehicles could increase from 59 km to 74 km by 2100. The adaptation scenario, which implemented nature-based solutions like porous pavements and green roofs, demonstrated the potential to reduce the EAD by approximately 12% to 17%, especially for more frequent flood events. However, they are insufficient to mitigate the effects of extreme events, which require a combination with traditional gray infrastructure for substantial risk reductions.

The findings were validated through a comparative analysis with the previous RESCCUE project in Barcelona, showing consistent trends in damage growth despite variations in modeling approaches and climate factors.

These results offer a robust evidence base for urban planners, emergency responders, and public administrations to prioritize resilience investments. By identifying specific high-risk clusters and demonstrating the cost-effectiveness of multiple adaptation measures, this research supports the development of targeted climate adaptation strategies to enhance urban resilience in this region.

Author Contributions: Conceptualization, À.d.l.C.-C. and B.R.; methodology, À.d.l.C.-C. and B.R.; software, À.d.l.C.-C. and B.R.; validation, À.d.l.C.-C. and B.R.; formal analysis, À.d.l.C.-C., S.P.-G., D.Y.-P. and B.R.; investigation, À.d.l.C.-C. and B.R.; resources, À.d.l.C.-C. and B.R.; data curation, À.d.l.C.-C., S.P.-G., D.Y.-P. and B.R.; writing—original draft preparation, À.d.l.C.-C.; writing—review and editing, B.R.; visualization, À.d.l.C.-C., S.P.-G. and D.Y.-P.; supervision, B.R.; project administration, B.R.; funding acquisition, À.d.l.C.-C. and B.R. All authors have read and agreed to the published version of the manuscript.

Funding: This publication was supported by The ICARIA project (Improving Climate Resilience of Critical Assets), funded by the European Commission through the Horizon Europe Programme, grant number 101093806 (https://cordis.europa.eu/project/id/101093806) and the program "Pla de Doctorats Industrials" (Generalitat de Catalunya). A.D.L.C-C also acknowledges the financial support provided by the Agència de Gestió d'Ajuts Universitaris i de Recerca (https://agaur.gencat.cat/en/inici/) through the Industrial Doctorate Plan of the Secretariat for Universities and Research Department of Business and Knowledge of the Government of Catalonia, under the Grant ID 2023-0030.

Institutional Review Board Statement: Not applicable.

Informed Consent Statement: Not applicable.

Data Availability Statement: Datasets used in the current study are available from the authors upon reasonable request.

Acknowledgments: The authors acknowledge the Fundación para la Investigación del Clima (FIC) and the ICARIA project for providing the climate data used in this study, and Francisco Espejo Gil, representing the Consorcio de Compensación de Seguros, for his continuous collaboration in the economic impact assessment of floods. This publication received support from the Industrial Doctorates Programme of the Department of Research and Universities of the Government of Catalunya.

Conflicts of Interest: The authors Àlex de la Cruz-Coronas, Sofia Pacho-Gómez and Daniel Yubero-Peña are affiliated with Climate Change & Resilience Unit, Veolia, Paseo de la Zona Franca 46–48, 08038, Barcelona, Spain. All authors declare that the research was conducted entirely in the absence of any commercial, financial, or personal relationships that could be construed as a potential conflict of interest.

References

1. IPCC. *Climate Change 2022—Impacts, Adaptation and Vulnerability: Working Group II Contribution to the Sixth Assessment Report of the Intergovernmental Panel on Climate Change*, 1st ed.; Cambridge University Press: Cambridge, UK, 2023.
2. Dodman, D.; Hayward, B.; Pelling, M.; Castan Broto, V.; Chow, W.; Chu, E.; Dawson, R.; Khirfan, L.; McPhearson, A.; Prakash, A.; et al. Cities, Settlements and Key Infrastructure. In *Climate Change 2022: Impacts, Adaptation and Vulnerability. Contribution of Working Group II to the Sixth Assessment Report of the Intergovernmental Panel on Climate Change*; IPCC: Geneva, Switzerland, 2022.
3. EEA. *European Climate Risk Assessment*; European Environmental Agency: Copenhagen, Demnark, 2024.
4. UN DESA. *World Urbanization Prospects: The 2018 Revision*; United Nations, Department of Economic and Social Affairs, Population Division: New York, NY, USA, 2019.
5. Hallegatte, S.; Green, C.; Nicholls, R.J.; Corfee-Morlot, J. Future Flood Losses in Major Coastal Cities. *Nat. Clim. Change* **2013**, *3*, 802–806. [CrossRef]
6. Jongman, B.; Ward, P.J.; Aerts, J.C.J.H. Global Exposure to River and Coastal Flooding: Long Term Trends and Changes. *Glob. Environ. Change* **2012**, *22*, 823–835. [CrossRef]
7. Pakati, S.S.; Shoko, C.; Dube, T. Integrated Flood Modelling and Risk Assessment in Urban Areas: A Review on Applications, Strengths, Limitations and Future Research Directions. *J. Hydrol. Reg. Stud.* **2025**, *61*, 102583. [CrossRef]

8. Romali, N.S.; Sulong, S.; Kawasaki, A. A Systematic Review of Flood Damage Assessment: Insight for the Data-Scarce Regions. *Water Resour. Manag.* **2025**, *39*, 4707–4734. [CrossRef]
9. Fornino, M. *A Multi-Country Study of Forward-Looking Economic Losses from Floods and Tropical Cyclones*; IMF Working Papers; International Monetary Fund: Washington, DC, USA, 2024; Volume 2024, 45p. [CrossRef]
10. Fox, S.; Agyemang, F.; Hawker, L.; Neal, J. Integrating Social Vulnerability into High-Resolution Global Flood Risk Mapping. *Nat. Commun.* **2024**, *15*, 3155. [CrossRef]
11. Allaire, M. Socio-Economic Impacts of Flooding: A Review of the Empirical Literature. *Water Secur.* **2018**, *3*, 18–26. [CrossRef]
12. Ghosh, M.; Ghosh, S.; Karmakar, S. Assessment of Flood Risk in a Coastal City Considering Multiple Socio-Economic Vulnerability Scenarios. In *Proceedings of IAHS*; Copernicus GmbH: Göttingen, Germany, 2024; Volume 386, pp. 299–306.
13. CLIMATE Adapt Population Characteristics in Potential Flood-Prone Areas. Available online: https://climate-adapt.eea.europa.eu/en/observatory/publications-data/analysis-data/exposure-to-potential-flood-prone-areas (accessed on 16 March 2026).
14. EEA Floods in Europe. Available online: https://discomap.eea.europa.eu/ClimatePreparedness2025/?page=Floods (accessed on 16 March 2026).
15. EEA. *Responding to Climate Change Impacts on Human Health in Europe: Focus on Floods, Droughts and Water Quality*; European Environment Agency Publications Office: Luxembourg, 2024.
16. EEA. *Economic Losses and Fatalities from Weather- and Climate-Related Events in Europe (Briefing No. 21/2021)*; European Environmental Agency: Copenhagen, Denmark, 2021.
17. EEA. *Urban Adaptation in Europe: How Cities and Towns Respond to Climate Change (Report No. 12/2020)*; European Environmental Agency: Copenhagen, Denmark, 2020.
18. Pastor-Escuredo, D.; Torres, Y.; Martínez-Torres, M.; Zufiria, P.J. Rapid Multi-Dimensional Impact Assessment of Floods. *Sustainability* **2020**, *12*, 4246. [CrossRef]
19. Hammond, M.J.; Chen, A.S.; Djordjević, S.; Butler, D.; Mark, O. Urban flood impact assessment: A state-of-the-art review. *Urban Water J.* **2015**, *14*, 14–26. [CrossRef]
20. Sañudo, E.; García-Feal, O.; Hagen, L.; Cea, L.; Puertas, J.; Montalvo, C.; Alvarado-Vicencio, R.; Hofmann, J. IberSWMM+: A High-Performance Computing Solver for 2D-1D Pluvial Flood Modelling in Urban Environments. *J. Hydrol.* **2025**, *651*, 132603. [CrossRef]
21. Leandro, J.; Chen, A.S.; Djordjević, S.; Savić, D.A. Comparison of 1D/1D and 1D/2D Coupled (Sewer/Surface) Hydraulic Models for Urban Flood Simulation. *J. Hydraul. Eng.* **2009**, *135*, 495–504. [CrossRef]
22. De Saint-Venant, A.J.C.B. Théorie Du Mouvement Non Permanent Des Eaux, Avec Application Aux Crues Des Rivières et à l'introduction Des Marées Dans Leur Lit. In *Comptes Rendus Hebdomadaires des Séances de l'Académie des Sciences*; Gauthier-Villars: Paris, France, 1871.
23. Chaudhry, M.H. *Open-Channel Flow*; Springer International Publishing: Cham, Switzerland, 2022.
24. Cea, L.; Costabile, P. Flood Risk in Urban Areas: Modelling, Management and Adaptation to Climate Change. A Review. *Hydrology* **2022**, *9*, 50. [CrossRef]
25. Russo, B.; Velasco, M.; Locatelli, L.; Sunyer, D.; Yubero, D.; Monjo, R.; Martínez-Gomariz, E.; Forero-Ortiz, E.; Sánchez-Muñoz, D.; Evans, B.; et al. Assessment of Urban Flood Resilience in Barcelona for Current and Future Scenarios. The RESCCUE Project. *Sustainability* **2020**, *12*, 5638. [CrossRef]
26. Martínez-Gomariz, E.; Locatelli, L.; Guerrero, M.; Russo, B.; Martínez, M. Socio-Economic Potential Impacts Due to Urban Pluvial Floods in Badalona (Spain) in a Context of Climate Change. *Water* **2019**, *11*, 2658. [CrossRef]
27. Lou, Y.; Wang, P.; Li, Y.; Zhang, Y.; Xie, B.; Hu, T. Projecting Urban Flood Risk through Hydrodynamic Modeling under Shared Socioeconomic Pathways. *J. Environ. Manag.* **2024**, *370*, 122647. [CrossRef] [PubMed]
28. Wang, M.; Fu, X.; Zhang, D.; Chen, F.; Liu, M.; Zhou, S.; Su, J.; Tan, S.K. Assessing Urban Flooding Risk in Response to Climate Change and Urbanization Based on Shared Socio-Economic Pathways. *Sci. Total Environ.* **2023**, *880*, 163470. [CrossRef] [PubMed]
29. Bachofer, F.; Wang, Z.; Huth, J.; Eisfelder, C.; Reimuth, A.; Kuenzer, C. Urban Growth Prediction along Shared Socioeconomic Pathways (SSPs) for Future Flood Exposure Risk Assessment: A Cross-Continental Analysis of Coastal Cities. *Anthr. Coasts* **2026**, *9*, 1. [CrossRef]
30. Yan, L.; Rong, H.; Yang, W.; Lin, J.; Zheng, C. A Novel Integrated Urban Flood Risk Assessment Approach Based on One-Two Dimensional Coupled Hydrodynamic Model and Improved Projection Pursuit Method. *J. Environ. Manag.* **2024**, *366*, 121910. [CrossRef]
31. Noh, S.J.; Lee, J.-H.; Lee, S.; Kawaike, K.; Seo, D.-J. Hyper-Resolution 1D-2D Urban Flood Modelling Using LiDAR Data and Hybrid Parallelization. *Environ. Model. Softw.* **2018**, *103*, 131–145. [CrossRef]
32. Jayawardane, P.; Rajapakse, L.; Siriwardana, C. Integrated Flood Risk Management for Urban Resilience: A Multi-Method Framework Combining Hazard Mapping, Hydrodynamic Modelling, and Economic Impact Assessment. *Resilient Cities Struct.* **2025**, *4*, 117–131. [CrossRef]

33. Ming, X.; Liang, Q.; Jiang, J. Large-Scale High-Resolution Hydrodynamic Modelling of Urban Floods: Some Practical Considerations. *J. Hydro-Environ. Res.* **2025**, *59*, 100655. [CrossRef]
34. Xing, Y.; Liang, Q.; Wang, G.; Ming, X.; Xia, X. City-Scale Hydrodynamic Modelling of Urban Flash Floods: The Issues of Scale and Resolution. *Nat. Hazards* **2019**, *96*, 473–496. [CrossRef]
35. De Moel, H.; Jongman, B.; Kreibich, H.; Merz, B.; Penning-Rowsell, E.; Ward, P.J. Flood Risk Assessments at Different Spatial Scales. *Mitig. Adapt. Strateg. Glob. Change* **2015**, *20*, 865–890. [CrossRef]
36. Bevacqua, E.; Maraun, D.; Vousdoukas, M.I.; Voukouvalas, E.; Vrac, M.; Mentaschi, L.; Widmann, M. Higher Probability of Compound Flooding from Precipitation and Storm Surge in Europe under Anthropogenic Climate Change. *Sci. Adv.* **2019**, *5*, eaaw5531. [CrossRef]
37. Ward, P.J.; Couasnon, A.; Eilander, D.; Haigh, I.D.; Hendry, A.; Muis, S.; Veldkamp, T.I.E.; Winsemius, H.C.; Wahl, T. Dependence between High Sea-Level and High River Discharge Increases Flood Hazard in Global Deltas and Estuaries. *Environ. Res. Lett.* **2018**, *13*, 084012. [CrossRef]
38. Qiang, Y.; He, J.; Xiao, T.; Lu, W.; Li, J.; Zhang, L. Coastal Town Flooding upon Compound Rainfall-Wave Overtopping-Storm Surge during Extreme Tropical Cyclones in Hong Kong. *J. Hydrol. Reg. Stud.* **2021**, *37*, 100890. [CrossRef]
39. IPCC. *Climate Change 2023: Synthesis Report. Contribution of Working Groups I, II and III to the Sixth Assessment Report of the Intergovernmental Panel on Climate Change*; Team, C.W., Lee, H., Romero, J., Eds.; IPCC: Geneva, Switzerland, 2023.
40. Moftakhari, H.R.; Salvadori, G.; AghaKouchak, A.; Sanders, B.F.; Matthew, R.A. Compounding Effects of Sea Level Rise and Fluvial Flooding. *Proc. Natl. Acad. Sci. USA* **2017**, *114*, 9785–9790. [CrossRef] [PubMed]
41. Ward, P.J.; Daniell, J.; Duncan, M.; Dunne, A.; Hananel, C.; Hochrainer-Stigler, S.; Tijssen, A.; Torresan, S.; Ciurean, R.; Gill, J.C.; et al. Invited Perspectives: A Research Agenda towards Disaster Risk Management Pathways in Multi-(Hazard-)Risk Assessment. *Nat. Hazards Earth Syst. Sci.* **2022**, *22*, 1487–1497. [CrossRef]
42. AMB. Plan Clima i Energia 2030. Barcelona. 2018. Available online: https://www.amb.cat/s/es/web/medi-ambient/sostenibilitat/canvi-climatic/pla-clima-energia-2030.html (accessed on 10 January 2026).
43. Tang, Y.; Sun, Y.; Han, Z.; Soomro, S.; Wu, Q.; Tan, B.; Hu, C. Flood Forecasting Based on Machine Learning Pattern Recognition and Dynamic Migration of Parameters. *J. Hydrol. Reg. Stud.* **2023**, *47*, 101406. [CrossRef]
44. Yi, S.; Yi, J. Reservoir-Based Flood Forecasting and Warning: Deep Learning versus Machine Learning. *Appl. Water Sci.* **2024**, *14*, 237. [CrossRef]
45. Leone, M.F.; Zuccaro, G.; De Gregorio, D.; Turchi, A.; Tedeschi, A.; Büegelmayer-Blaschek, M.; Sfetsos, A.; Zarikos, I.; Coronas, A.D.L.C.; Russo, B. A Holistic Asset-Level Modelling Framework for a Comprehensive Multi-Hazard Risk/Impact Assessment: Insights from the ICARIA Project. *Int. J. Disaster Risk Reduct.* **2025**, *119*, 105319. [CrossRef]
46. UNDRR. *Sendai Framework for Disaster Risk Reduction 2015–2030*; UNDRR: Geneva, Switzerland, 2015; p. 37.
47. ICGC. Visor Cartogràfic de Catalunya ICGC. Available online: https://visors.icgc.cat/appdownloads/ (accessed on 8 April 2026).
48. De La Cruz-Coronas, A.; Pacho, S.; Büegelmayer-Blaschek, M.; Hasel, K.; Berg, R.; Havlik, D.; Duro, R.; Zarikos, I.; Pradell, P.; Cantó, N.; et al. ICARIA Deliverable 4.2: Trial Assessment. 2026. Available online: https://www.icaria-project.eu/downloads/#publications (accessed on 1 February 2026).
49. Ajuntament de Barcelona. Pla Direcotr Integral de Sanejament de La Ciutat de Barcelona—PDISBA: Estudi de Pluges 2019. Available online: https://bcnroc.ajuntament.barcelona.cat/jspui/handle/11703/119275 (accessed on 12 October 2025).
50. Paradinas Blázquez, C.; Büegelmayer-Blaschek, M.; Galiano Sánchez, L.; Redolat Negro, D.; Prado López, C.; Hasel, K.; Züger, J.; Lampert, J.; Thiele, P. *ICARIA Deliverable 1.2: Climate Projections and Hazard Scenarios*; European Commission: Brussels, Belgium, 2024; p. 210.
51. Catastro de España Sede Electrónica Del Catastro. Available online: https://www1.sedecatastro.gob.es/Cartografia/mapa.aspx?buscar=S (accessed on 8 April 2026).
52. Martínez-Gomariz, E.; Forero-Ortiz, E.; Guerrero-Hidalga, M.; Castán, S.; Gómez, M. Flood Depth–Damage Curves for Spanish Urban Areas. *Sustainability* **2020**, *12*, 2666. [CrossRef]
53. INE INEbase—Demografía y Población. Available online: https://www.ine.es/dyngs/INEbase/categoria.htm?c=Estadistica_P&cid=1254734710984 (accessed on 8 April 2026).
54. OpenStreetMap OpenStreetMap. Available online: https://www.openstreetmap.org/ (accessed on 8 April 2026).
55. Autodesk. *InfoWorks ICM Ultimate, version 2026.2*; Autodesk: San Rafael, CA, USA, 2025.
56. Chen, A.; Evans, B.; De La Cruz-Coronas, A.; Russo, B.; Büegelmayer-Blaschek, M.; Zarios, I. ICARIA Deliverable 2.4: ICARIA Multi-Hazards Modelling Tools and Application Guidelines—Version 2. 2025. Available online: https://mission-adaptation-portal.ec.europa.eu/icaria_en (accessed on 1 February 2026).
57. Aguilera-Vidal, M.; Sanuy, M.; Ortego, M.I.; Jiménez, J.A. Rainfall and Wave Storms Interdependence in the Western Spanish Mediterranean Coast. *J. Hydrol. Reg. Stud.* **2025**, *62*, 102873. [CrossRef]

58. Sanuy, M.; Rigo, T.; Jiménez, J.A.; Llasat, M.C. Classifying Compound Coastal Storm and Heavy Rainfall Events in the North-Western Spanish Mediterranean. *Hydrol. Earth Syst. Sci.* **2021**, *25*, 3759–3781. [CrossRef]
59. Sanuy, M.; Peña, J.C.; Assimenidis, S.; Jiménez, J.A. Synoptic Weather Patterns Conducive to Compound Extreme Rainfall–Wave Events in the NW Mediterranean. *Hydrol. Earth Syst. Sci.* **2024**, *28*, 283–302. [CrossRef]
60. Insa Ferrándiz, J. Study and Assessment of Adaptive Measures to the Impact of Coastal Flooding Hazard on the Llevant Main Sewer (Barcelona, Spain). Bachelor's Thesis, Universitat Politècnica de Catalunya, Barcelona, Spain, 2025.
61. Ortiz, A.; Velasco, M.J.; Esbri, O.; Medina, V.; Russo, B. The Economic Impact of Climate Change on Urban Drainage Master Planning in Barcelona. *Sustainability* **2020**, *13*, 71. [CrossRef]
62. Estrella, S.; Olivares, G.; Russo, B.; Sánchez-Juny, M. Mezclas bituminosas porosas en el contexto de los SUDS: Revisión y perspectivas. *Ing. Agua* **2025**, *29*, 179–201. [CrossRef]
63. Olivares-Cerpa, G.; Russo, B.; Martínez-Puentes, M.; Bladé, E.; Sanz-Ramos, M. "SUDS-lineales" para reducir el riesgo de inundación considerando escenarios de Cambio Climático. *Ing. Agua* **2022**, *26*, 77–90. [CrossRef]
64. Ajuntament de Barcelona Barcelona. *Nature Plan 2021–2030*; Ajuntament de Barcelona: Barcelona, Spain, 2020.
65. Khromova, S.; Busse, S.; Benati, G.; Herreros Cantis, P.; Segura-Barrero, R.; Ventura, S.; Eckelman Matthew, J.; Villalba Méndez, G.; Langemeyer, J. Title: From Runoff to Resilience: Exploring Multifunctional Nature-Based Solutions for Sustainable Urban Stormwater Management. *Urban For. Urban Green.* **2026**, *120*, 129431. [CrossRef]
66. Velasco, M.; Russo, B.; Cabello, À.; Termes, M.; Sunyer, D.; Malgrat, P. Assessment of the Effectiveness of Structural and Nonstructural Measures to Cope with Global Change Impacts in Barcelona. *J. Flood Risk Manag.* **2016**, *11*, S55–S68. [CrossRef]
67. Locatelli, L.; Guerrero, M.; Russo, B.; Martínez-Gomariz, E.; Sunyer, D.; Martínez, M. Socio-Economic Assessment of Green Infrastructure for Climate Change Adaptation in the Context of Urban Drainage Planning. *Sustainability* **2020**, *12*, 3792. [CrossRef]
68. Russo, B.; Gómez, M.; Macchione, F. Pedestrian Hazard Criteria for Flooded Urban Areas. *Nat. Hazards* **2013**, *69*, 251–265. [CrossRef]
69. Ward, P.J.; de Moel, H.; Aerts, J.C.J.H. How Are Flood Risk Estimates Affected by the Choice of Return-Periods? *Nat. Hazards Earth Syst. Sci.* **2011**, *11*, 3181–3195. [CrossRef]

Disclaimer/Publisher's Note: The statements, opinions and data contained in all publications are solely those of the individual author(s) and contributor(s) and not of MDPI and/or the editor(s). MDPI and/or the editor(s) disclaim responsibility for any injury to people or property resulting from any ideas, methods, instructions or products referred to in the content.